

1 **Evolution of antibody immunity following Omicron BA.1 breakthrough infection**

2
3 **Authors:** Chengzi I. Kaku^{1,2}, Tyler N. Starr^{3,4}, Panpan Zhou^{2,5,6}, Haley L. Dugan¹, Paul Khalifé¹,
4 Ge Song^{2,5,6}, Elizabeth R. Champney¹, Daniel W. Mielcarz⁷, James C. Geoghegan¹, Dennis R.
5 Burton^{2,5,6,8}, Raiees Andrabi^{2,5,6}, Jesse D. Bloom^{3,9,10}, Laura M. Walker^{11*}

6
7 **Affiliations:**

8 ¹ Adimab, LLC, Lebanon, NH 03766, USA.

9 ² Department of Immunology and Microbiology, The Scripps Research Institute, La Jolla, CA
10 92037, USA.

11 ³ Basic Sciences Division, Fred Hutchinson Cancer Center, Seattle, WA 98109, USA.

12 ⁴ Department of Biochemistry, University of Utah School of Medicine, Salt Lake City, UT 84112

13 ⁵ IAVI Neutralizing Antibody Center, The Scripps Research Institute, La Jolla, CA 92037, USA.

14 ⁶ Consortium for HIV/AIDS Vaccine Development (CHAVD), The Scripps Research Institute,
15 La Jolla, CA 92037, USA.

16 ⁷ Dartmouth Cancer Center, Geisel School of Medicine, Lebanon NH 03766, USA.

17 ⁸ Ragon Institute of Massachusetts General Hospital, Massachusetts Institute of Technology, and
18 Harvard University, Cambridge, MA 02139, USA.

19 ⁹ Department of Genome Sciences, University of Washington, Seattle, WA 98109, USA.

20 ¹⁰ Howard Hughes Medical Institute, Seattle, WA 98109, USA.

21 ¹¹ Invivyd Inc., Waltham, MA 02451, USA.

22
23 * Corresponding author. E-mail: lwalker@invivid.com (L.M.W.)

24
25 **Abstract:**

26
27 Understanding the evolution of antibody immunity following heterologous SAR-CoV-2
28 breakthrough infection will inform the development of next-generation vaccines. Here, we
29 tracked SARS-CoV-2 receptor binding domain (RBD)-specific antibody responses up to six
30 months following Omicron BA.1 breakthrough infection in mRNA-vaccinated individuals.
31 Cross-reactive serum neutralizing antibody and memory B cell (MBC) responses declined by
32 two- to four-fold through the study period. Breakthrough infection elicited minimal de novo
33 Omicron-specific B cell responses but drove affinity maturation of pre-existing cross-reactive
34 MBCs toward BA.1. Public clones dominated the neutralizing antibody response at both early
35 and late time points, and their escape mutation profiles predicted newly emergent Omicron
36 sublineages. The results demonstrate that heterologous SARS-CoV-2 variant exposure drives the
37 evolution of B cell memory and suggest that convergent neutralizing antibody responses
38 continue to shape viral evolution.

39
40 **Main text:**

41
42 The emergence and global spread of the SARS-CoV-2 Omicron BA.1 variant in late 2021
43 resulted in the largest surge in COVID-19 caseloads to date (1). While currently available
44 COVID-19 vaccines induced high levels of protection against pre-Omicron variants, the
45 extensive immune evasiveness of Omicron resulted in significantly reduced vaccine efficacy and
46 durability following both primary and booster immunization (2–5). Moreover, antigenically

47 drifted sub-lineages of Omicron (e.g. BA.2, BA.2.12.1, BA.4/5, BA.2.75, BA.2.75.2, and
48 BA.4.6) continue to emerge and supplant prior sub-variants (4, 6). The high prevalence of
49 Omicron breakthrough infections led to the development and emergency use authorization of
50 Omicron variant-based booster mRNA vaccines, despite limited immunogenicity and efficacy
51 data in humans (2, 7). Thus, there is an urgent need to understand if and how secondary exposure
52 to antigenically divergent variants, such as Omicron, shape SARS-CoV-2-specific B cell
53 memory.

54
55 We and others have previously reported that the acute antibody response following Omicron
56 BA.1 breakthrough infection is dominated by re-activated memory B cells induced by mRNA
57 vaccination (8–11). In support of these findings, preliminary data from clinical trials evaluating
58 the immunogenicity of variant-based booster vaccines demonstrated that BA.1-containing
59 mRNA vaccines induce a modest improvement in peak serum neutralizing responses compared
60 with ancestral Wuhan-1 immunization (12). Although these studies provide evidence for
61 “original antigenic sin” in the early B cell response following Omicron breakthrough infection, if
62 and how this response evolves over time remains unclear. To address these questions, we
63 longitudinally profiled SARS-CoV-2-specific serological and memory B responses in mRNA-
64 vaccinated donors up to six months following BA.1 breakthrough infection.

65
66 We initially characterized the antibody response to SARS-CoV-2 in a cohort of seven mRNA-
67 1273 vaccinated donors 14 to 27 days (median = 23 days) after BA.1 breakthrough infection (8).
68 To study the evolution of this response, we obtained blood samples from six of the seven
69 participants at a follow-up appointment four to six months (median = 153 days) post-infection
70 (Fig. 1A, Table S1). Three of the six donors experienced infection after two-dose mRNA-1273
71 vaccination while the remaining three donors were infected after a third booster dose. None of
72 the donors reported a second breakthrough infection between the two sample collection time
73 points.

74
75 To evaluate serum neutralization breadth and potency, we tested the plasma samples for
76 neutralizing activity against SARS-CoV-2 D614G, emergent variants (BA.1, BA.2, BA.4/5,
77 BA.2.75, Beta, and Delta), and the more evolutionarily divergent sarbecovirus SARS-CoV, in a
78 murine-leukemia virus (MLV)-based pseudovirus assay. Paired comparisons within each
79 participant revealed that serum neutralizing titers against D614G declined by a median of 4.8-
80 fold at 5- to 6-months post-infection relative to those observed within one-month post-infection
81 (Fig. 1B). Correspondingly, we observed lower serum neutralizing titers against Omicron sub-
82 variants (2.8 to 3.9-fold, respectively), Beta (1.6-fold), Delta (3.8-fold), and SARS-CoV (3.1-
83 fold) at the 5- to 6-month time point relative to the early time point (Fig. 1B). Despite this
84 waning of neutralizing antibody titers over time, all of the donor sera displayed detectable
85 neutralizing activity against all of the SARS-CoV-2 variants tested at the 5-6 month time point
86 (median titers ranging from 117 to 552) (Fig. 1C). Notably, titers remained within 3-fold of that
87 observed for D614G for all variants except BA.4/5, which showed the greatest degree of escape
88 from serum neutralizing antibodies (5.5-fold reduction from D614G), consistent with published
89 serological studies (4, 5). Furthermore, the fold reduction in serum neutralizing titer for SARS-
90 CoV-2 VOCs relative to D614G remained similar at both time points, suggesting maintained
91 serum neutralization breadth over time (Fig. 1D). We observed minimal cross-neutralizing
92 activity against SARS-CoV (median titer = 21) in all donors, suggesting that serum

93 neutralization breadth remained limited to SARS-CoV-2 variants (Fig. 1C). We conclude that
94 serum neutralizing titers wane over the course 6-months following Omicron BA.1 breakthrough
95 infection but nevertheless remain at detectable levels across a diverse range of SARS-CoV-2
96 variants through 6 months.

97
98 Next, we assessed the magnitude and cross-reactivity of the antigen-specific B cell response via
99 flow cytometric enumeration of B cells stained with differentially labeled wildtype (Wuhan-1;
100 WT) and BA.1 RBD tetramers (Fig. 2A, Fig. S1A). At the 5-6-month time point, total RBD-
101 reactive B cells (WT and/or BA.1-reactive) and WT/BA.1 cross-reactive B cells comprised a
102 median of 0.44% (ranging 0.12-2.53%) and 0.37% (ranging 0.12-2.53%) of class-switched (IgG⁺
103 or IgA⁺) B cells, respectively (Fig. 2B, 2C, Fig. S1A). Thus, 86% (ranging 69-100%) of all
104 RBD+ class-switched B cells at 5-6 months post-infection displayed BA.1/WT cross-reactivity,
105 compared with 75% at 1-month post-infection (ranging 65-81%) (Fig. 2D, Fig. S2).
106 Correspondingly, WT-specific B cells decreased from 25% of all RBD+ class-switched B cells at
107 1 month to 11% at 5-6 months (Fig. 2D, Fig. S2). Consistent with the waning of serum
108 neutralizing titers over time, we also observed a modest but significant decline (1.1 to 3.7-fold)
109 in the frequencies of WT/BA.1 cross-reactive B cells at 5-6 months relative to the 1-month time
110 point (Fig. 2C). At the late time point, we also detected the emergence of a BA.1-specific B cell
111 population (average = 3% of class-switched B cells) in 3 of the 6 individuals, although the
112 magnitude of this response varied widely among individuals (ranging from 1-18%) (Fig. 2D, Fig.
113 S2). In summary, Omicron BA.1 breakthrough infection induces a WT/BA.1 cross-reactive B
114 cell response at early time points post-infection and this response only modestly declines over
115 the course of 6 months.

116
117 To compare the molecular characteristics of antibodies isolated at early and late time points
118 following BA.1 breakthrough infection, we single-cell sorted 71 to 110 class-switched RBD-
119 reactive B cells from four of the five previously studied donors (donors IML4042, IML4043,
120 IML4044, IML4045) at 139 to 170 days after breakthrough infection and expressed a total of 363
121 natively paired antibodies as full-length IgGs (Fig. S1B) (8). Similar to the antibodies
122 characterized from the acute time point, the newly isolated antibodies primarily recognized both
123 WT and BA.1 RBD antigens (73-97%), exhibited a high degree of clonal diversity, and
124 displayed preferential usage of certain VH germline genes (*IGHV1-46*, *1-69*, *3-13*, *3-53*, *3-66*, *3-*
125 *9*, and *4-31* germline genes at both time points) (Fig. 2E, Fig. S3 and S4). The level of SHM in
126 the cross-reactive antibodies increased from a median of 9 VH nucleotide substitutions at 1-
127 month to 11 VH nucleotide substitutions by 5-6 months, potentially suggesting affinity
128 maturation in secondary germinal centers (Fig. 2F). Consistent with their higher levels of SHM,
129 the antibodies isolated at 5-6 months displayed 1.7-fold improved binding to BA.1 (median KD
130 = 1.3 nM) and 2-fold reduced binding affinity to the WT RBD (median K_D = 1.0 nM) relative to
131 early antibodies, suggesting maturation towards Omicron BA.1 at the expense of WT affinity
132 (Fig. 3A and 3B). These changes in binding recognition resulted in the late antibodies showing
133 more balanced affinity profiles compared to the early antibodies (Fig 3B). For example, the
134 majority of antibodies (73%) isolated at the late time point exhibited WT and BA.1 RBD
135 affinities within two-fold of each other compared to only 24% of early antibodies (Fig. 3C).

136
137 To determine whether the improvement in binding affinity for BA.1 translated into enhanced
138 neutralization potency, we assessed the antibodies for neutralizing activity against WT and BA.1

139 using a pseudovirus assay. Fifty-one percent and 42% of WT/BA.1 cross-binding antibodies
140 isolated from the 1-month and 5-6-month time point, respectively, cross-neutralized D614G and
141 BA.1 with $IC_{50} < 2 \mu\text{g/ml}$. Overall, the neutralizing antibodies displayed approximately 2-fold
142 lower potency against D614G at the late time point relative to the acute time point, consistent
143 with the observed reduction in WT RBD affinity over time (Fig. 3D and 3E). As expected, the
144 improvement in BA.1 binding affinities over time translated into an overall improvement in
145 neutralization potency (Fig. 3E). Approximately 16% of antibodies isolated at 5-6 months
146 displayed neutralization $IC_{50s} < 0.01 \mu\text{g/ml}$ compared to only 2% of antibodies isolated at the
147 earlier time point (Fig. S5). As a result, forty-one percent of the neutralizing antibodies isolated
148 at 6 months exhibited more potent activity against BA.1 relative to D614G, compared to only 7%
149 of the acute neutralizing antibodies (Fig 3F). In summary, cross-reactive antibody responses
150 induced following BA.1 breakthrough infection evolve toward increased BA.1 affinity and
151 neutralization potency for at least 6 months post-infection.

152

153 Although the vast majority of antibodies isolated at the 5-6-month time point displayed
154 WT/BA.1 cross-reactive binding, we identified a limited number of BA.1-specific antibodies in
155 all four donors, comprising 1% to 15% of total RBD-specific antibodies (median = 4%) (Fig.
156 S3). In contrast, we only detected BA.1-specific antibodies in a single donor at the acute time
157 point (Fig. S3). Furthermore, unlike the BA.1-specific antibodies isolated at the early time point,
158 which lacked somatic mutations, the BA.1-specific antibodies identified at 5-6 months displayed
159 SHM levels similar to those of cross-reactive antibodies (median = 11 VH nucleotide
160 substitutions) (Fig. 2F). Forty percent of BA.1-specific antibodies isolated at the late time point
161 neutralized BA.1, with IC_{50s} ranging from 0.002 to 0.089 $\mu\text{g/ml}$, and none of the antibodies
162 displayed detectable neutralizing activity against D614G (Fig. S6). Thus, BA.1 breakthrough
163 infection induces a limited and delayed de novo Omicron-specific B cell response that undergoes
164 affinity maturation over time.

165

166 To further explore the breadth of both WT/BA.1 cross-reactive and BA.1-specific neutralizing
167 antibodies, we evaluated their binding reactivities with a panel of recombinant RBDs encoding
168 mutations present in SARS-CoV-2 variants BA.2, BA.4/5, Beta, and Delta, and the more
169 antigenically divergent SARS-CoV. D614G/BA.1 cross-neutralizing antibodies displayed 2.4-
170 fold reduced affinity for the WT RBD and 3.4-fold improved affinity for the BA.1 RBD relative
171 to early neutralizing antibodies, consistent with the pattern observed for all WT/BA.1 cross-
172 binding antibodies (Fig. 4A, Fig. 3A-C). Furthermore, the WT/BA.1 cross-reactive antibodies
173 isolated at 6 months broadly recognized other SARS-CoV-2 variants, except for BA.4/5, which
174 was associated with a ≥ 5 -fold loss in affinity for 57% (68/120) of the WT/BA.1 neutralizing
175 antibodies (Fig. 4A, Fig. S7). Importantly, the 5-6-month antibodies displayed higher affinity
176 binding to all Omicron sub-variants and Beta relative to the early antibodies, suggesting that the
177 increased affinity to BA.1 also improved breadth of reactivity against other variants (Fig. 4A). In
178 support of this finding, a significantly higher proportion (40%) of neutralizing antibodies isolated
179 at 6 months displayed high affinity ($K_D < 10\text{nM}$) binding to all five variants tested compared
180 with early antibodies (22%) (Fig. 4B). Furthermore, antibodies isolated at the late time point
181 displayed smaller differences in binding affinity against BA.1, BA.2, BA.4/5 and the early Beta
182 and Delta variants relative to early antibodies (Fig. 4C). In contrast to the WT/BA.1 cross-
183 reactive antibodies, the BA.1-specific neutralizing antibodies displayed limited breadth, with
184 only 50% of these antibodies maintaining binding to BA.2 and none of the antibodies showing

185 reactivity with WT, BA.4/5, Beta, or Delta (Fig. S6). We conclude that BA.1 breakthrough
186 infection results in an overall broadening of the anti-SARS-CoV-2 neutralizing antibody
187 repertoire.

188
189 Among neutralizing antibodies isolated at both time points, we observed significant over-
190 representation of four IGHV germline genes (*IGHV1-69*, *IGHV3-53/3-66*, and *IGHV3-9*) (8) (Fig
191 S8A). At the 5-6-month time point, over half (54%) of the neutralizing antibodies were encoded
192 by one of these four germlines, with one-third of these antibodies utilizing *IGHV1-69* (Fig. 4D,
193 Fig. S8). We previously found that BA.1-neutralizing *IGHV1-69* antibodies isolated from the
194 early time point preferentially paired with the light chain germline *IGLV1-40* and targeted an
195 antigenic site overlapping that of the class 3 antibody COV2-2130 and non-overlapping with the
196 ACE2 binding site (8). Similarly, 69% of *IGHV1-69* antibodies isolated at 5-6 months paired
197 with the *IGLV1-40* germline and the majority (80%) failed to compete with ACE2 for binding
198 (Fig. S9A and C). Likewise, >90% of *IGHV3-9* antibodies identified from both time points
199 recognized a non-ACE2-competitive binding site, although unlike *IGHV1-69* antibodies, *IGHV3-9*
200 antibodies recognize an epitope overlapping S309 and REGN10987 as well as COV2-2130,
201 suggesting a distinct mode of binding from *IGHV1-69* antibodies (Fig. S9C) (8). Lastly, *IGHV3-53/66*
202 antibodies isolated from both time points were characterized by short HCDR3s (median =
203 11 to 12 nucleotide substitutions) compared with baseline HCDR3 lengths (median = 15
204 substitutions) and displayed competitive binding with the ACE2 receptor (Fig. S9B and C).
205 Thus, convergent antibody classes dominated the neutralizing antibody response at both early
206 and late time points following BA.1 breakthrough infection, suggesting little to no change in B
207 cell immunodominance hierarchy over time.

208
209 Given the dominance of these public clonotypes in BA.1 breakthrough infection donors, we
210 sought to determine their escape mutations in the BA.1 background. We randomly selected one
211 to two antibodies belonging to each convergent germline and performed deep mutational
212 scanning (DMS) analysis using a library encoding all possible amino acid substitutions from
213 BA.1 (Fig. S10A) (13). Antibodies encoded by *IGHV3-53* (ADI-75733) and *IGHV3-66* (ADI-
214 75732) displayed similar escape profiles, consistent with their shared sequence features and
215 competitive binding profiles (Fig. 4E and Fig. S10C) (8). RBD positions N460 and F486, which
216 are mutated in emergent variants (N460K in B.2.75, BA.2.75.2, BN.1, and BQ.1; F486S in
217 BA.2.75.2; and F486V in BA.4/5, BA.4.6, and BQ.1.1), were associated with binding escape
218 from *IGHV3-53/66* antibodies (Fig. 4F and Fig. 10C). *IGHV1-69* and *IGHV3-9* antibodies both
219 showed reduced binding to RBDs incorporating mutations at positions 344-349, 356, 452-453,
220 468, and 490. Notably, residues R346, K356, L452, and F490 are mutated across evolutionarily
221 diverse Omicron sub-lineages, including BA.4.6 (R346T, L452R), BA.4/5 (L452R), BA.2.12.1
222 (L452Q), BJ.1 (R346T, F490V), BN.1 (R346T, K356T, F490S), and BQ.1.1 (R346T, L452R)
223 (Fig. 4F and Fig. S10C). Consistent with these escape profiles, *IGHV1-69* and *IGHV3-9* class
224 antibodies displayed reduced binding to BA.2.12.1 and BA.4/5 relative to early Omicron
225 variants, likely due to the unique L452Q/R mutations present in these variants compared with
226 BA.1 and BA.2 (Fig. 4G). Consistent with DMS-based predictions, both BA.2.75 and BA.4/5
227 RBDs displayed increased binding resistance to *IGHV3-53/66* antibodies (Fig. 4F and 4G). Thus,
228 convergent D614G/BA.1 cross-neutralizing antibodies recognize epitopes commonly mutated in
229 recently emerging Omicron sub-variants, providing a molecular explanation for the high degree

230 of antigenic convergence observed in recent Omicron sub-variant evolution and their increased
231 level of immune evasion relative to BA.1.

232
233 In summary, BA.1 breakthrough infection in mRNA-vaccinated individuals induces broadly
234 neutralizing serological and MBC responses that persist for at least six months after infection,
235 supporting real-world studies showing that BA.1 breakthrough infection provides protection
236 against symptomatic BA.1, BA.2, and BA.5 infection for at least 5-6 months (14–16).
237 Furthermore, although the acute B cell response following breakthrough infection is primarily
238 mediated by recall of cross-reactive vaccine-induced MBCs, these MBC clones accumulate
239 somatic mutations and evolve increased breadth and potency for at least 6 months following
240 infection. Although this enhanced neutralization breadth and potency was not reflected in the
241 serum antibody response, it is possible that a second heterologous exposure may broaden the
242 serological repertoire by activating these affinity matured MBCs, akin to the improved serum
243 neutralization breadth observed following mRNA booster vaccination (17, 18). Nevertheless, our
244 data indicate that infection or vaccination with antigenically divergent SARS-CoV-2 variants
245 may provide long-term benefits by broadening pre-existing anti-SARS-CoV-2 B cell memory.
246

247 Finally, we found that convergent classes of neutralizing antibodies dominated the BA.1
248 breakthrough response at both early and late time points, reminiscent of the antibody response
249 elicited following primarily infection or vaccination with early ancestral SARS-CoV-2 strains
250 (19–21). The sustained prevalence of public clones that target residues frequently mutated in
251 emerging Omicron subvariants suggests that this response is the driving force behind the
252 continued antigenic drift of Omicron. Thus, in contrast to current approaches to the design of
253 universal vaccines for certain highly antigenically variable viruses, such as HIV and influenza,
254 which aim to focus the neutralizing response on a limited number of relatively conserved
255 epitopes, the development of “variant-proof” COVID-19 vaccines may require a different
256 strategy: engineering of spike-based immunogens that induce a diversity of neutralizing
257 antibodies targeting numerous co-dominant epitopes, with the goal of limiting convergent
258 immune pressure and therefore constraining viral evolution (22–24).
259

260 **References and Notes:**

- 261 1. WHO Coronavirus (COVID-19) Dashboard | WHO Coronavirus (COVID-19) Dashboard
262 With Vaccination Data, (available at <https://covid19.who.int/>).
- 263 2. H. F. Tseng *et al.*, *Nat. Med.* **28**, 1063–1071 (2022).
- 264 3. S. Y. Tartof *et al.*, *Lancet Respir. Med.* **10**, 689–699 (2022).
- 265 4. Q. Wang *et al.*, *Nature*. **608**, 603–608 (2022).
- 266 5. A. Tuekprakhon *et al.*, *Cell*. **185**, 2422–2433.e13 (2022).
- 267 6. P. Qu *et al.*, *BioRxiv* (2022), doi:10.1101/2022.08.14.503921.
- 268 7. Coronavirus (COVID-19) Update: FDA Authorizes Moderna, Pfizer-BioNTech Bivalent
269 COVID-19 Vaccines for Use as a Booster Dose | FDA, (available at
270 <https://www.fda.gov/news-events/press-announcements/coronavirus-covid-19-update-fda-authorizes-moderna-pfizer-biontech-bivalent-covid-19-vaccines-use>).
- 272 8. C. I. Kaku *et al.*, *Sci. Immunol.* **7**, eabq3511 (2022).
- 273 9. J. Quandt *et al.*, *Sci. Immunol.* **7**, eabq2427 (2022).
- 274 10. Z. Wang *et al.*, *BioRxiv* (2022), doi:10.1101/2022.08.11.503601.
- 275 11. Y. Cao *et al.*, *BioRxiv* (2022), doi:10.1101/2022.09.15.507787.

276 12. S. Chalkias *et al.*, *N. Engl. J. Med.* (2022), doi:10.1056/NEJMoa2208343.
277 13. T. N. Starr *et al.*, *BioRxiv* (2022), doi:10.1101/2022.09.20.508745.
278 14. H. Chemaitletta *et al.*, *medRxiv* (2022), doi:10.1101/2022.02.24.22271440.
279 15. J. Malato *et al.*, *N. Engl. J. Med.* **387**, 953–954 (2022).
280 16. D.-Y. Lin *et al.*, *N. Engl. J. Med.* (2022), doi:10.1056/NEJMc2209371.
281 17. F. Muecksch *et al.*, *Nature*. **607**, 128–134 (2022).
282 18. W. F. Garcia-Beltran *et al.*, *Cell*. **185**, 457–466.e4 (2022).
283 19. D. F. Robbiani *et al.*, *Nature*. **584**, 437–442 (2020).
284 20. C. O. Barnes *et al.*, *Nature*. **588**, 682–687 (2020).
285 21. Z. Wang *et al.*, *Nature*. **592**, 616–622 (2021).
286 22. A. Lanzavecchia, A. Frühwirth, L. Perez, D. Corti, *Curr. Opin. Immunol.* **41**, 62–67
287 (2016).
288 23. A. B. Ward, I. A. Wilson, *Curr. Opin. Immunol.* **65**, 50–56 (2020).
289 24. P. D. Kwong, J. R. Mascola, *Immunity*. **48**, 855–871 (2018).
290 25. B. Briney, A. Inderbitzin, C. Joyce, D. R. Burton, *Nature*. **566**, 393–397 (2019).
291 26. T. F. Rogers *et al.*, *Science*. **369**, 956–963 (2020).
292 27. A. Z. Wec *et al.*, *Proc Natl Acad Sci USA*. **117**, 6675–6685 (2020).
293 28. R. D. Gietz, R. H. Schiestl, *Nat. Protoc.* **2**, 31–34 (2007).
294 29. M. I. J. Raybould, A. Kovaltsuk, C. Marks, C. M. Deane, *Bioinformatics*. **37**, 734–735
295 (2021).
296 30. M. Sakharkar *et al.*, *Sci. Immunol.* **6** (2021), doi:10.1126/sciimmunol.abg6916.
297

298 **Acknowledgements:**

299 We thank T. Boland for assistance with sequence analysis. We acknowledge E. Krauland, J.
300 Nett, M. Vasquez, and C.G. Rappazzo for helpful comments on the manuscript. We also thank
301 the Flow Cytometry and Genomics Shared Facilities at Fred Hutchinson Cancer Center. All IgGs
302 were sequenced by Adimab's Molecular Core and produced by the High-Throughput Expression
303 group. **Funding:** T.N.S. is supported by the NIAID/NIH (K99AI166250). D.M. is funded by the
304 NCI Cancer Center Support Grant (5P30 CA023108-41). D.R.B. is funded by the Bill and
305 Melinda Gates Foundation INV-004923 and by the James B. Pendleton Charitable Trust. J.D.B.
306 is supported by the NIH/NIAID (R01AI141707) and is an Investigator of the Howard Hughes
307 Medical Institute. **Author contributions:** C.I.K. and L.M.W. conceived and designed the study.
308 D.M. supervised and performed clinical sample collection and processing. C.I.K. designed and
309 performed B cell analyses. C.I.K. and P.K. performed single B cell sorting. C.I.K., P.Z., P.K.,
310 and H.L.D. performed pseudovirus neutralization assays. T.N.S. designed and performed
311 antibody deep mutational scanning analyses. C.I.K. and E.R.C. performed biolayer
312 interferometry assays. C.I.K., H.L.D., and G.S. conducted antibody sequence analyses. C.I.K.,
313 T.N.S., H.L.D., J.C.G., D.R.B., R.A., J.D.B., and L.M.W. analyzed the data. C.I.K. and L.M.W.
314 wrote the manuscript, and all authors reviewed and edited the paper. **Competing interests:**
315 C.I.K. is a former employee and holds shares in Adimab. LLC. P.K., H.L.D., E.R.C., and J.C.G.
316 are current employees and hold shares in Adimab LLC. L.M.W. is an employee and holds shares
317 in Invivyd Inc. T.N.S. and J.D.B. consult with Apriori Bio. J.D.B. has consulted for Moderna and
318 Merck on viral evolution and epidemiology. D.R.B. is a consultant for IAVI, Invivyd, Adimab,
319 Mabloc, VosBio, Nonigenex, and Radian. C.I.K. and L.M.W. are inventors on a provisional
320 patent application describing the SARS-CoV-2 antibodies reported in this work. T.N.S. and
321 J.D.B. may receive a share of intellectual property revenue as inventors on Fred Hutchinson

322 Cancer Center–optioned technology and patents related to deep mutational scanning of viral
323 proteins. The other authors declare that they have no competing interests. **Data and materials**
324 **availability:** Omicron BA.1 yeast-display deep mutational scanning libraries are available from
325 Addgene (accession # 1000000187). Complete computational pipeline with intermediate and
326 final data files is available from GitHub: https://github.com/jbloomlab/SARS-CoV-2-RBD_Omicron_MAP_Adimab. All other data needed to evaluate the conclusions in the paper
327 are present in the paper or the Supplementary Materials. IgGs are available from L.M.W. under a
328 material transfer agreement from Invivyd Inc.
329

330

331 **Supplementary Materials**

332 Materials and Methods

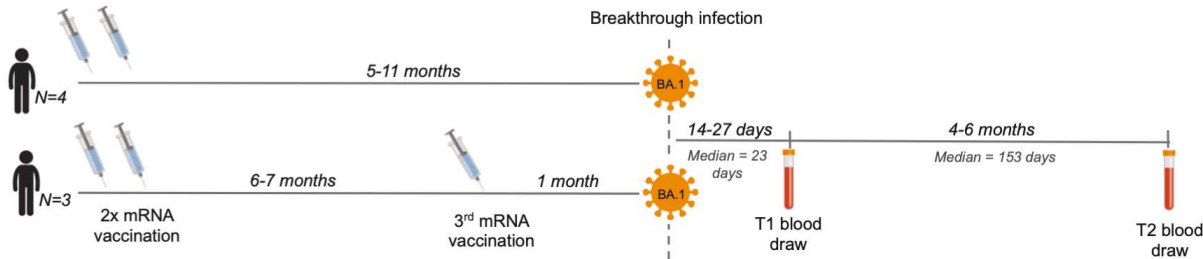
333 Figures S1 – S10

334 Table S1

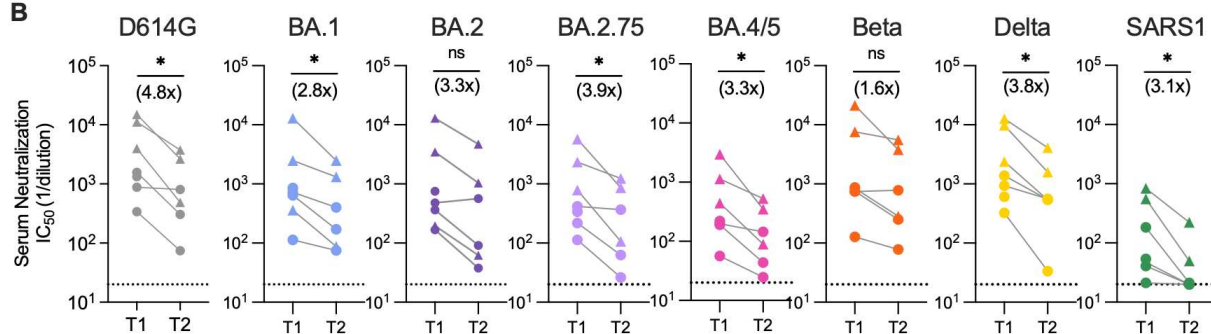
335 References 25 – 30

336 **Main Text Figures:**

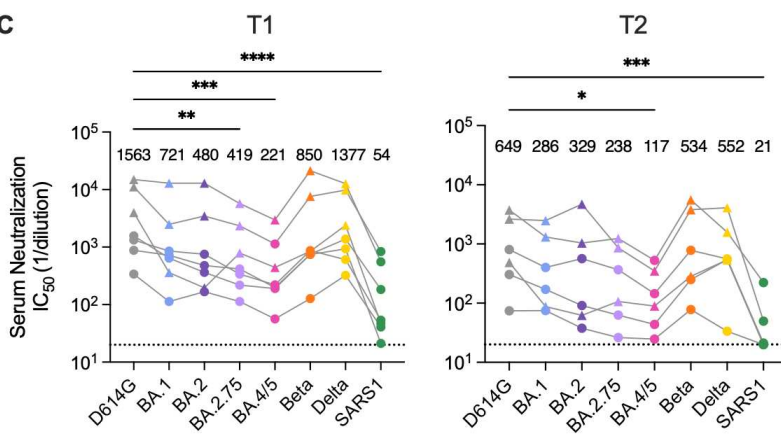
A



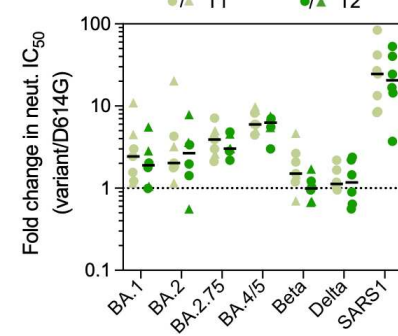
B



C



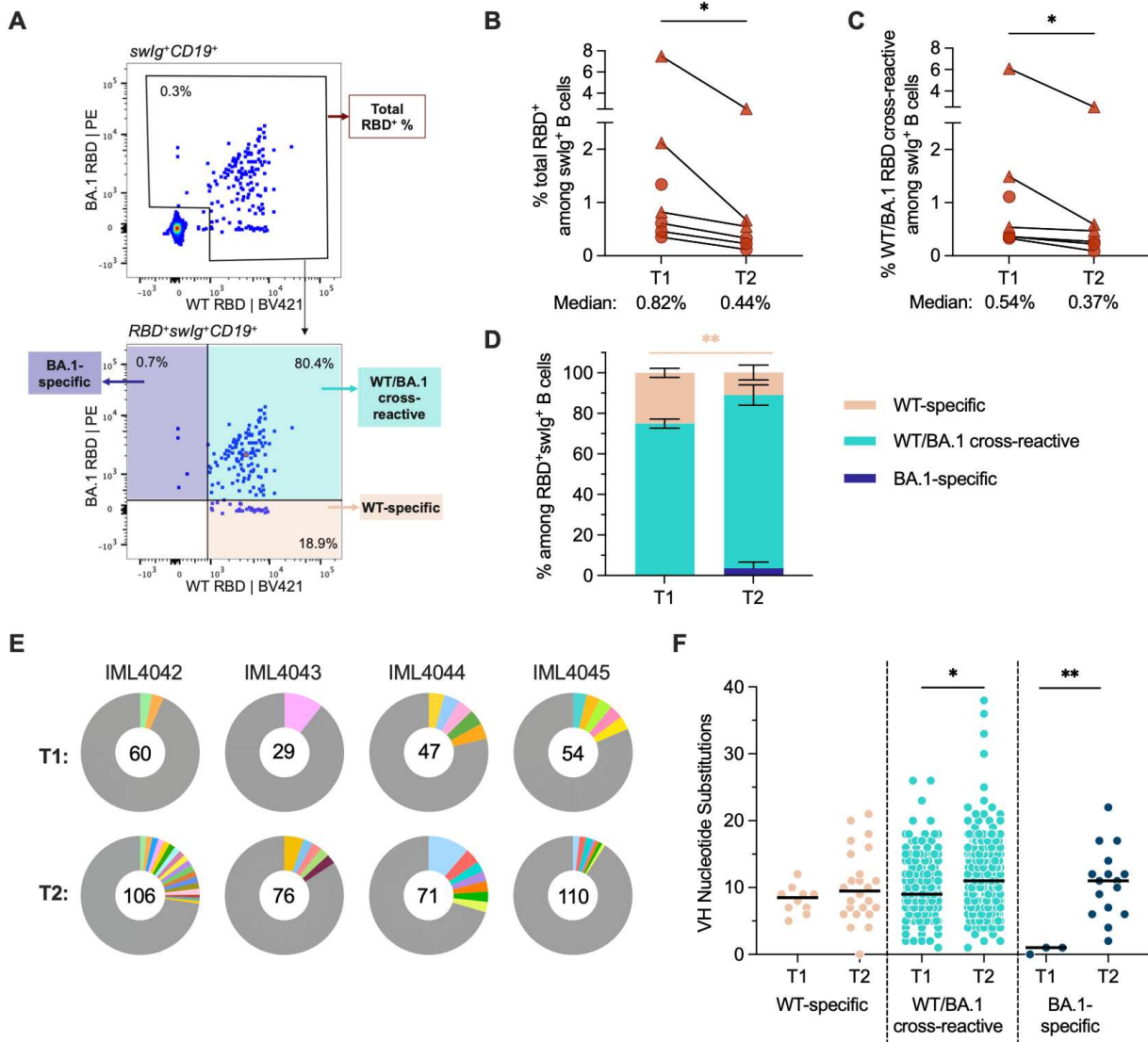
D



337

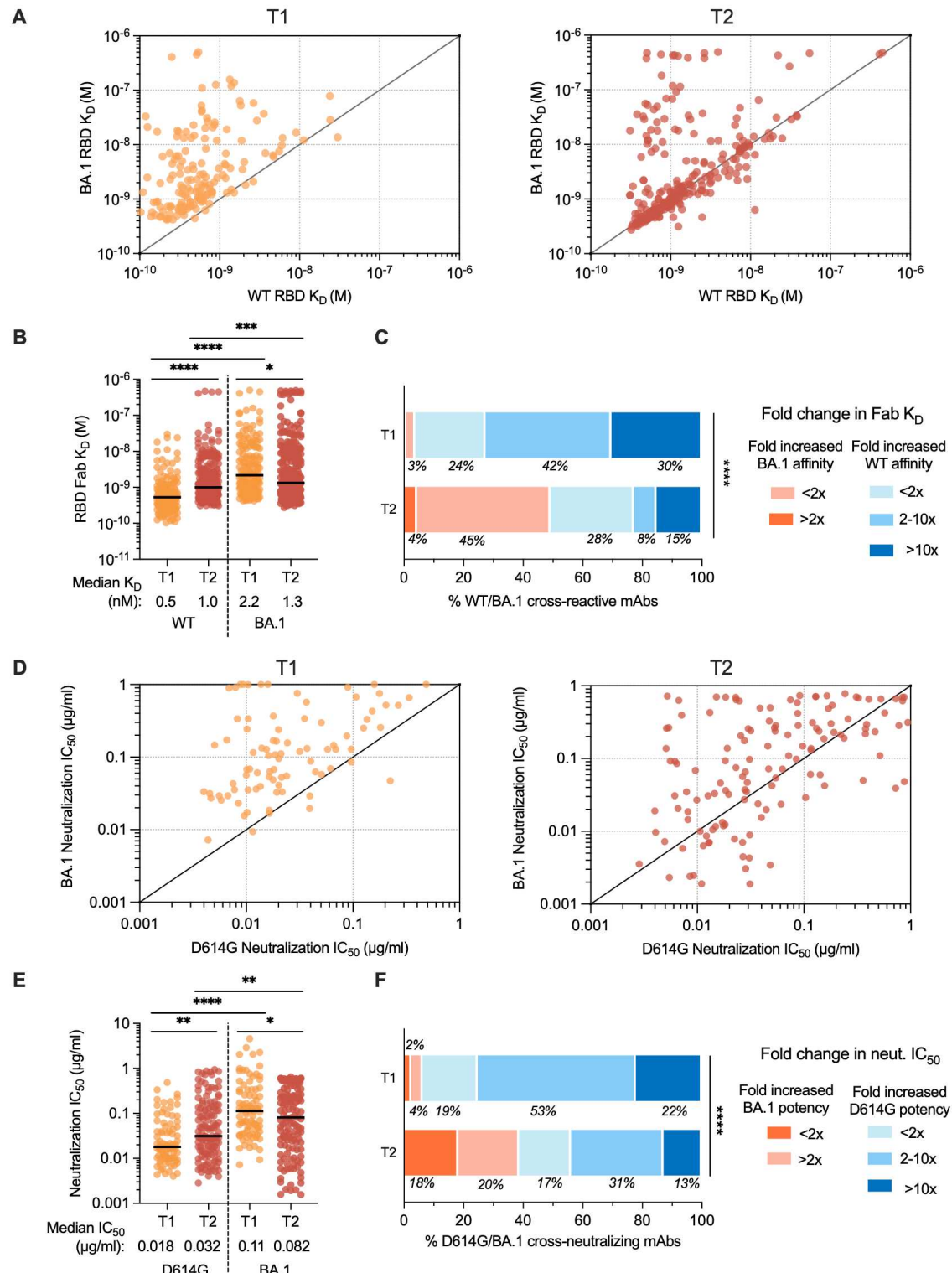
338 **Figure 1. Serum neutralizing antibody responses induced following BA.1 breakthrough**
 339 **infection. (A)** Timeline of vaccination, BA.1 breakthrough infection, and sample collections. **(B)**
 340 Paired analysis of serum neutralizing activity against SARS-CoV-2 D614G and BA.1, BA.2,
 341 BA.2.75, BA.4/5, Beta, and Delta variants, and SARS-CoV (SARS1) at 1-month (T1) and 5-6-
 342 month (T2) time points, as determined via a MLV-based pseudovirus neutralization assay.
 343 Connected data points represent paired samples for each donor, and the median fold change in
 344 serum titer between the two time points is shown in parentheses. Dotted lines represent the lower
 345 limit of detection of the assay. **(C)** Serum neutralizing titers against SARS-CoV-2 variants and
 346 SARS-CoV in samples collected at (left) 1-month and (right) 5-6-month post-breakthrough
 347 infection for each donor. Median titers are shown above the data points. Dotted lines represent
 348 the lower limit of detection of the assay. **(D)** Fold change in serum neutralizing titers for the
 349 indicated SARS-CoV-2 variants and SARS-CoV relative to SARS-CoV-2 D614G at early (T1)
 350 and late (T2) time points. Black bars represent median fold changes. Dotted line indicates no
 351 change in IC₅₀. Breakthrough infection donors infected after two-dose mRNA vaccination (n = 4)

352 are shown as circles and those infected after a third mRNA dose (n = 3) are shown as triangles.
353 One two-dose vaccinated breakthrough donor was lost to follow-up at the second time point.
354 Statistical comparisons were determined by (B) Wilcoxon matched-pairs signed rank test, (C)
355 Friedman's one-way ANOVA with Dunn's multiple comparisons, or (D) mixed model ANOVA.
356 * $P < 0.05$; ** $P < 0.01$; **** $P < 0.0001$; ns, not significant.



357
358 **Figure 2. SARS-CoV-2 RBD-specific memory B cell responses following BA.1**
359 **breakthrough infection.** (A) Representative fluorescence-activated cell sorting strategy
360 used to enumerate frequencies of (top) total (WT+BA.1) RBD-reactive B cells among class-
361 switched (IgG⁺ or IgA⁺) CD19⁺ B cells and (bottom) WT-specific, BA.1-specific, and WT/BA.1
362 cross-reactive B cells among total RBD-reactive, class-switched (IgG⁺ or IgA⁺) CD19⁺ B cells.
363 (B-C) Frequencies of (B) total RBD-reactive or (C) WT/BA.1 RBD cross-reactive B cells among
364 class-switched CD19⁺ B cells at 1-month (T1) and 5-6-month (T2) time points. Connected data
365 points represent paired samples for each donor. Donors infected after two-dose mRNA
366 vaccination (n = 4) are shown as circles and those infected after a third mRNA dose (n = 3) are
367 shown as triangles. One two-dose vaccinated breakthrough donor was censored at the second
368 time point. (D) Mean proportions of RBD-reactive, class-switched B cells that display WT-
369 specific, BA.1-specific or WT/BA.1-cross-reactive binding at each time point. Error bars
370 indicate standard error of mean. (E) Clonal lineage analysis of RBD-directed antibodies isolated
371 from four donors at the early (T1) and late (T2) time points. Clonally expanded lineages (defined
372 as antibodies with the same heavy and light chain germlines, same CDR3 lengths, and ≥ 80%
373 CDRH3 sequence identity) are represented as colored slices. Each colored slice represents a

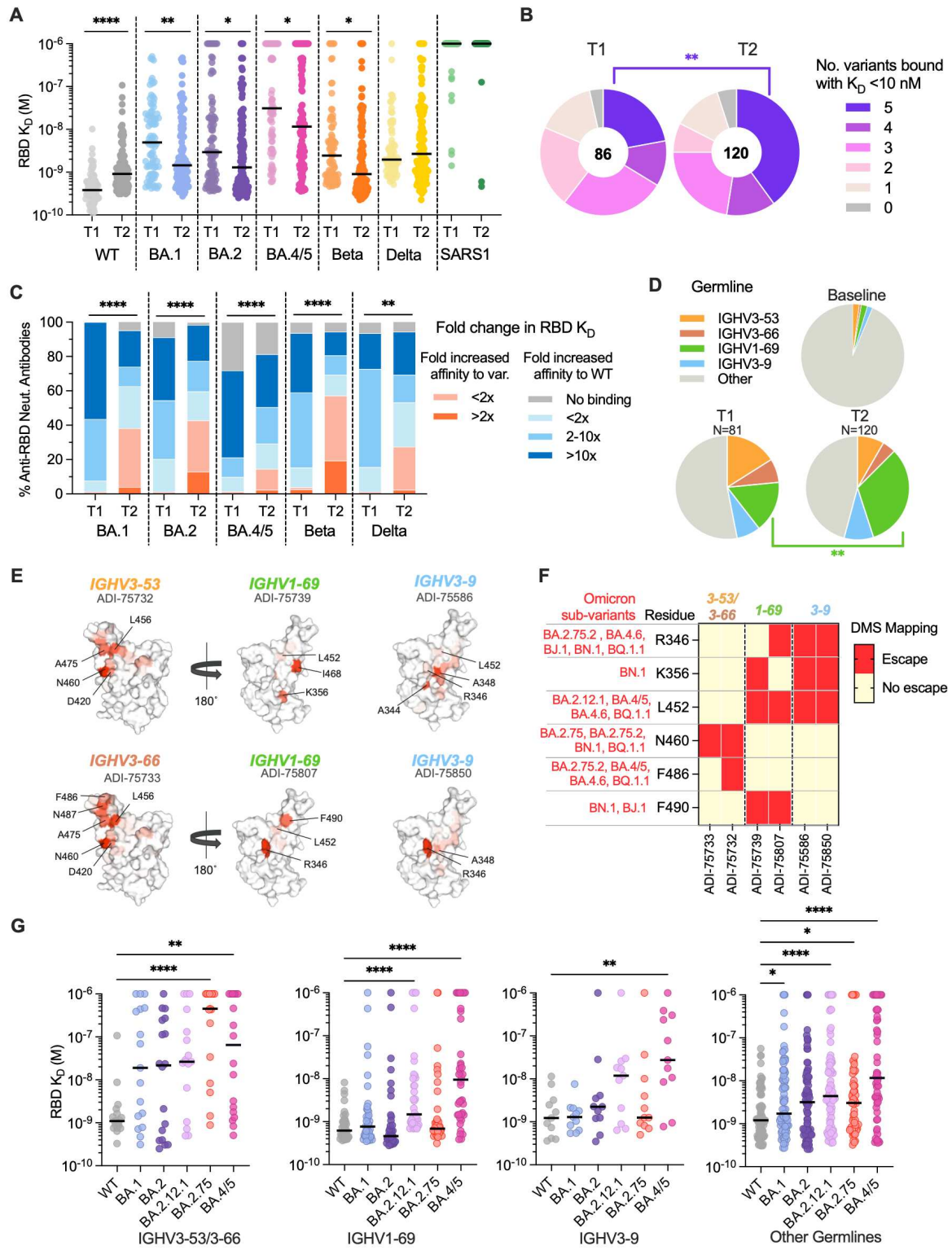
374 clonal lineage with the size of the slice proportional to the lineage size. Unique clones are
375 combined into a single gray segment. The number of antibodies is shown in the center of each
376 pie. Three of the donors (IML4042, IML4043, and IML4044) experienced BA.1 breakthrough
377 infection following two-dose mRNA vaccination and the remaining donor (IML4045) was
378 infected after a booster immunization. **(F)** Levels of somatic hypermutation, as determined by
379 the number of nucleotide substitutions in the variable heavy (VH) region, at the early and late
380 time points among WT-specific, WT/BA.1 cross-reactive, and BA.1-specific antibodies.
381 Medians are shown by black bars. Statistical significance was determined by (B and C)
382 Wilcoxon matched-pairs signed rank test or (D and F) Mann-Whitney U test. swIg⁺, class-
383 switched immunoglobulin. PE, phycoerythrin; * $P < 0.05$; ** $P < 0.01$.



384

385 **Figure 3. Binding and neutralizing properties of RBD-directed antibodies induced by BA.1**
 386 **breakthrough infection. (A-B)** Fab binding affinities of WT/BA.1 cross-reactive antibodies for
 387 recombinant WT and BA.1 RBD antigens, as measured by BLI, are plotted as bivariate for
 388 antibodies derived from (left) 1-month and (right) 5-6-month time points in (A) and summarized
 389 as a column dot plot in (B). Median affinities are indicated by black bars and shown below data

390 points. **(C)** Proportions of WT/BA.1 cross-reactive antibodies at each time point that show
391 increased affinity for the BA.1 RBD relative to WT (red shades) or increased affinity for WT
392 RBD (blue shades). Values represent the percentage of antibodies belonging to each of the
393 indicated categories. **(D-E)** Neutralizing activities of cross-binding antibodies against SARS-
394 CoV-2 D614G and BA.1, as determined by an MLV-based pseudovirus neutralization assay.
395 IC₅₀ values are plotted in (D) as bivariate for antibodies isolated from (left) 1-month and (right)
396 5-6-month tie points and summarized as column dot plots in (E). Median IC₅₀ values are
397 indicated by black bars and shown below data points. **(F)** Proportions of WT/BA.1 cross-
398 neutralizing antibodies at each time point that show increased neutralizing potency against BA.1
399 (red shades) or D614G (blue shades). Values represent the percentage of antibodies belonging to
400 each of the indicated categories. Statistical comparisons were determined by (B and E) multiple
401 Mann-Whitney U tests without adjustment for multiplicity across time points and Wilcoxon
402 matched-pairs rank tests within each time point or (C and F) Mann-Whitney U test. IC₅₀, 50%
403 inhibitory concentration; K_D, equilibrium dissociation constant; *P < 0.05; **P < 0.01; ***P <
404 0.0001.



405

406 **Figure 4. Breadth of D614G/BA.1 cross-neutralizing antibodies at early and late time**
 407 **points following BA.1 breakthrough infection. (A)** Fab binding affinities of D614G/BA.1
 408 cross-neutralizing antibodies isolated at 1-month (T1) and 5-6-month (T2) time points for
 409 recombinant SARS-CoV-2 variant RBDs and the SARS-CoV RBD, as determined by BLI. Black
 410 bars represent medians. **(B)** Pie charts showing the proportions of antibodies derived from (left)

411 early and (right) late time points that bound the indicated number of SARS-CoV-2 variant RBDs
412 with Fab K_D s < 10 nM. The total number of antibodies is shown in the center of each pie. **(C)**
413 Proportions of D614G/BA.1 cross-neutralizing antibodies with the indicated fold changes in Fab
414 binding affinities for recombinant SARS-CoV-2 variant RBDs relative to the WT RBD. **(D)** Pie
415 charts showing frequencies of the indicated convergent germline genes among D614G/BA.1
416 cross-neutralizing antibodies isolated at early (T1) and late (T2) timelines. Germline gene
417 frequencies observed in baseline human antibody repertoires (upper right) are shown for
418 comparison (25). **(E)** Structural projections of binding escape mutations determined for the
419 indicated convergent antibodies using deep mutational scanning analysis of yeast-displayed
420 SARS-CoV-2 BA.1 RBD mutant libraries. The RBD surface is colored by a gradient ranging
421 from no escape (white) to strong escape (red) at each site. See Fig. S10 for additional details. **(F)**
422 Heatmap summarizing convergent antibody escape mutations present in the indicated SARS-
423 CoV-2 Omicron sub-lineages. **(G)** Fab binding affinities of convergent antibodies utilizing the
424 indicated germline genes for SARS-CoV-2 WT and Omicron sub-variant RBD antigens, as
425 measured by BLI. Black bars indicate median affinities. Statistical comparisons were determined
426 by (A and C) Kruskal-Wallis test with Holms corrected multiple pairwise comparisons, (B and
427 D) Fisher's exact test, or (G) Kruskal-Wallis test with subsequent Dunn's multiple comparisons
428 with WT. K_D , equilibrium dissociation constant; * $P < 0.05$; ** $P < 0.01$; *** $P < 0.001$; **** $P <$
429 0.0001.

430
431
432
433
434
435
436
437
438

Supplementary Materials for

Evolution of antibody immunity following Omicron BA.1 breakthrough infection

442
443 Chengzi I. Kaku, Tyler N. Starr, Panpan Zhou, Haley L. Dugan, Paul Khalifé, Ge Song,
444 Elizabeth R. Champney, Daniel W. Mielcarz, James C. Geoghegan, Dennis R. Burton, Raiees
445 Andrabi, Jesse D. Bloom, Laura M. Walker*

*Correspondence to: L.M.W. lwalker@invivyd.com

449 This PDF file includes:

450 Materials and Methods 451 Figs. S1 to S10 452 Table S1

453 **Materials and Methods**

454

455 **Human subjects and blood sample collection.**

456 Seven BA.1 breakthrough infected participants were recruited to participate in this study
457 with informed consent under the healthy donor protocol D10083, Immune Monitoring Core
458 (DartLab) Laboratory at Dartmouth-Hitchcock Hospital, as previously described (8). Briefly,
459 participants experienced breakthrough infection after two- or three-dose mRNA vaccination
460 (BNT162b2 and/or mRNA-1273). Venous blood was collected at two time points, an early visit
461 at 14 to 27 days (T1) and a late visit 139 to 170 days (T2) after their first SARS-CoV-2 test.
462 Participants had no documented history of SARS-CoV-2 infection prior to vaccination or
463 between the two blood draw time points. Clinical and demographic characteristics of
464 breakthrough infection donors are shown in Table S1. Plasma and peripheral blood mononuclear
465 cell (PBMC) samples were isolated using a Ficoll 1077 (Sigma) gradient, as previously described
466 (8).

467

468 **Plasmid Design and Construction.**

469 Plasmids expressing spike proteins of SARS-CoV-2 variants and SARS-CoV were
470 ordered as gene block fragments (IDT) and cloned into a mammalian expression vector for
471 MLV-based pseudovirus production as previously described (26). All SARS-CoV-2 variant
472 spikes and the SARS-CoV spike were C-terminally truncated by 19-amino acids or 28-amino
473 acids, respectively, to increase infectious titers. The SARS-CoV S sequence was retrieved from
474 ENA (AAP13441). SARS-CoV-2 variants contain the following mutations from the Wuhan-Hu-
475 1 sequence (Genbank: NC_045512.2):

- 476 • D614G: D614G
- 477 • Beta: D80A, D215G, Δ242-244, K417N, E484K, N501Y, D614G, A701V
- 478 • Delta: T19R, G142D, Δ156-157, R158G, L452R, T478K, D614G, P681R, D950N
- 479 • BA.1: A67V, Δ69-70, T95I, G142D/Δ143-145, Δ211/L212I, ins214EPE, G339D,
480 S371L, S373P, S375F, K417N, N440K, G446S, S477N, T478K, E484A, Q493R,
481 G496S, Q498R, N501Y, Y505H, T547K, D614G, H655Y, N679K, P681H, N764K,
482 D796Y, N856K, Q954H, N969K, L981F
- 483 • BA.2: T19I, L24S, Δ25-27, G142D, V213G, G339D, S371F, S373P, S375F, T376A,
484 D405N, R408S, K417N, N440K, S477N, T478K, E484A, Q493R, Q498R, N501Y,
485 Y505H, D614G, H655Y, N679K, P681H, N764K, D796Y, Q954H, N969K
- 486 • BA.4/5: T19I, L24S, Δ25-27, Δ69-70, G142D, V213G, G339D, S371F, S373P,
487 S375F, T376A, D405N, R408S, K417N, N440K, L452R, S477N, T478K, E484A,
488 F486V, Q498R, N501Y, Y505H, D614G, H655Y, N679K, P681H, N764K, D796Y,
489 Q954H, N969K
- 490 • BA.2.75: T19I, L24S, Δ25-27, G142D, K147E, W152R, F157L, I210V, V213G,
491 G339H, G257S, S371F, S373P, S375F, T376A, D405N, R408S, K417N, N440K,
492 G446S, N460K, S477N, T478K, E484A, Q498R, N501Y, Y505H, D614G, H655Y,
493 N679K, P681H, N764K, D796Y, Q954H, N969K

494

495 **SARS-CoV-2 pseudovirus generation.**

496 Single-cycle infectious MLVs pseudotyped with spike proteins of SARS-CoV-2 variants
497 and SARS-CoV were generated as previously described (26). Briefly, HEK293T cells were
498 seeded at a density of 0.5 million cells/ml in 6-well tissue culture plates and the next day,

499 transfected using Lipofectamine 2000 (ThermoFisher Scientific) with the following plasmids: 1)
500 0.5 μ g per well of pCDNA3.3 encoding SARS-CoV-2 spike with a 19-amino acid truncation at
501 the C-terminus, 2) 2 μ g per well of MLV-based luciferase reporter gene plasmid (Vector
502 Builder), and 3) 2 μ g per well of of MLV gag/pol (Vector Builder). MLV particles were
503 harvested 48 h post-transfection, aliquoted, and stored at -80 °C for neutralization assays.
504

505 **Pseudovirus neutralization assay.**

506 MLV pseudovirus neutralization assays for serum and monoclonal antibodies were
507 performed as previously described (8). Briefly, 56 °C heat-inactivated sera or antibodies were
508 serially diluted in 50 μ l MEM/EBSS media supplemented with 10% fetal bovine serum (FBS)
509 and incubated with 50 μ l of MLV viral stock for 1 h at 37 °C. Following incubation, antibody-
510 virus mixtures were added to previously seeded HeLa-hACE2 reporter cells (BPS Bioscience Cat
511 #79958). Infection was allowed to occur for 48 h at 37 °C. Infection was measured by lysing
512 cells with Luciferase Cell Culture Lysis reagent (Promega) and detecting luciferase activity using
513 the Luciferase Assay System (Promega) following manufacturer's protocols. Infectivity was as
514 quantified by relative luminescence units (RLUs) and the percentage neutralization was
515 calculated as $100 * (1 - [RLU_{sample} - RLU_{background}] / [RLU_{isotype control mAb} - RLU_{background}])$.
516 Neutralization IC₅₀ was interpolated from curves fitted using four-parameter non-linear
517 regression in GraphPad Prism (version 9.3.1).
518

519 **FACS analysis of SARS-CoV-2 S-specific B cell responses.**

520 Antigen-specific B cells were detected using recombinant biotinylated antigens tetramerized with
521 fluorophore-conjugated streptavidin (SA), as previously described (8). Briefly, Avitag
522 biotinylated WT RBD (Acro Biosystems, Cat #SPD-C82E8) and Avitag biotinylated BA.1 RBD
523 (Acro Biosystems, Cat # SPD-C82E4) were mixed in 4:1 molar ratios with SA-BV421
524 (BioLegend) and SA-phycoerythrin (PE; Invitrogen), respectively, and allowed to incubate for
525 20 min on ice. Unbound SA sites were subsequently quenched using 5 μ l of 2 μ M Pierce biotin
526 (ThermoFisher Scientific). Approximately 10 million PBMCs were stained with tetramerized
527 RBDs (25 nM each); anti-human antibodies anti-CD19 (PE-Cy7; Biolegend), anti-CD3 (PerCP-
528 Cy5.5; Biolegend), anti-CD8 (PerCP-Cy5.5; Biolegend), anti-CD14 (PerCP-Cy5.5; Invitrogen),
529 and anti-CD16 (PerCP-Cy5.5; Biolegend); and 50 μ l Brilliant Stain Buffer (BD BioSciences)
530 diluted in FACS buffer (2% BSA/1 mM EDTA in 1X PBS). 200 μ l of staining reagents were
531 added to each PBMC sample and incubated for 15 min on ice. After one wash with FACS buffer,
532 cells were stained in a mixture of propidium iodide and anti-human antibodies anti-IgG (BV605;
533 BD Biosciences), anti-IgA (FITC; Abcam), anti-CD27 (BV510; BD Biosciences), and anti-
534 CD71 (APC-Cy7; Biolegend). Following 15 min of incubation on ice, cells were washed two
535 times with FACS buffer and analyzed using a BD FACS Aria II (BD BioSciences).
536

537 For sorting of RBD-specific, class-switched B cells, PBMCs that react with either WT
538 and/or BA.1 RBD tetramers among CD19⁺CD3⁻CD8⁻CD14⁻CD16⁻PI⁻ and IgG⁺ or IgA⁺ cells
539 were single-cell index sorted into 96-well polystyrene microplates (Corning) containing 20 μ l
540 lysis buffer per well [5 μ l of 5X first strand SSIV cDNA buffer (Invitrogen), 1.25 μ l
541 dithiothreitol (Invitrogen), 0.625 μ l of NP-40 (Thermo Scientific), 0.25 μ l RNaseOUT
542 (Invitrogen), and 12.8 μ l dH₂O]. Plates briefly centrifuged and then frozen at -80 °C before PCR
543 amplification.
544

Amplification and cloning of antibody variable genes.

545 Antibody variable gene fragments (VH, Vk, V λ) were amplified by RT-PCR as described
546 previously (27). Briefly, cDNA was synthesized using randomized hexamers and SuperScript IV
547 enzyme (ThermoFisher Scientific). cDNA was subsequently amplified by two rounds of nested
548 PCRs, with the second cycle of nested PCR adding 40 base pairs of flanking DNA homologous
549 to restriction enzyme-digested *S. cerevisiae* expression vectors to enable homologous
550 recombination during transformation. PCR-amplified variable gene DNA was mixed with
551 expression vectors and chemically transformed into competent yeast cells via the lithium acetate
552 method (28). Yeast were plated on selective amino acid drop-out agar plates and individual yeast
553 colonies were picked for sequencing and recombinant antibody expression.

554

555 **Expression and purification of IgG and Fab molecules.**

556 Antibodies were expressed as human IgG1 via *S. cerevisiae* cultures, as described
557 previously (27). Briefly, yeast cells were grown in culture for 6 days for antibody production,
558 before collecting IgG-containing supernatant by centrifugation. IgGs were subsequently purified
559 by protein A-affinity chromatography and eluted using 200 mM acetic acid/50 mM NaCl (pH
560 3.5). The pH was then neutralized using 1/8th volume of 2 M Hepes (pH 8.0). Fab fragments
561 were cleaved from full-length IgG by incubating with papain for 2 h at 30 °C before terminating
562 the reaction using iodoacetamide. Fab fragments were purified from the mixture of digested
563 antibody Fab ad Fc fragments using a two-step chromatography system: 1) Protein A agarose
564 was used to remove Fc fragments and undigested IgG, and 2) Fabs in the flow-through were
565 further purified using CaptureSelect™ IgG-CH1 affinity resin (ThermoFisher Scientific) and
566 eluted from the column using 200 mM acetic acid/50 mM NaCl (pH 3.5). Fab solutions were pH-
567 neutralized using 1/8th volume 2 M Hepes (pH 8.0).

568

569 **Binding affinity measurements by biolayer interferometry.**

570 Antibody binding kinetics were measured by biolayer interferometry (BLI) using a
571 FortéBio Octet HTX instrument (Sartorius). All steps were performed at 25 °C and at an orbital
572 shaking speed of 1000 rpm, and all reagents were formulated in PBSF buffer (PBS with 0.1%
573 w/v BSA). To measure monovalent binding affinities against SARS-CoV-2 RBD variants and
574 SARS-CoV S, recombinant RBDs of SARS-CoV-2 WT (Acro Biosystems, Cat #SPD-C52H3),
575 Beta (Acro Biosystems, Cat #SPD-C52Hp), Delta (Acro Biosystems, Cat #SPD-C52Hh), BA.1
576 (Acro Biosystems, Cat #SPD-C522f), BA.2 (Acro Biosystems, Cat#SPD-C522g), BA.4/5 (Acro
577 Biosystems, Cat#SPD-C522r), and SARS-CoV (Sino Biological, Cat #40150-V08B2) were
578 biotinylated using EZ-Link™ Sulfo-NHS-LC-Biotin (Thermo Scientific) following
579 manufacturer's recommendations to achieve an average of 4 biotins per RBD molecule.
580 Biotinylated antigens were diluted (100 nM) in PBSF and loaded onto streptavidin biosensors
581 (Sartorius) to a sensor response of 1.0-1.2 nm and then allowed to equilibrate in PBSF for a
582 minimum of 30 min. After a 60 s baseline step in PBSF, antigen-loaded sensors were exposed
583 (180 s) to 100 nM Fab and then dipped (420 s) into PBSF to measure any dissociation of the
584 antigen from the biosensor surface. Fab binding data with detectable binding responses (>0.1
585 nm) were aligned, inter-step corrected (to the association step) and fit to a 1:1 binding model
586 using the FortéBio Data Analysis Software (version 11.1).

587

588 **ACE2 competition by biolayer interferometry.**

589 Antibody binding competition with recombinant human ACE2 receptor (Sino Biological,
590 Cat# 10108-H08H) was determined by BLI using a ForteBio Octet HTX (Sartorius). All binding

591 steps were performed at 25 °C and at an orbital shaking speed of 1000 rpm. All reagents were
592 formulated in PBSF (1X PBS with 0.1% w/v BSA). IgGs (100 nM) were captured onto anti-
593 human IgG capture (AHC) biosensors (Molecular Devices) to a sensor response of 1.0 nm-1.4
594 nm, and then soaked (20 min) in an irrelevant IgG1 solution (0.5 mg/ml) to block remaining Fc
595 binding sites. Next, sensors were equilibrated for 30 min in PBSF and then briefly exposed (90 s)
596 to 300 nM of ACE2 to assess any potential cross interactions between sensor-loaded IgG and
597 ACE2. Sensors were allowed to baseline (60 s) in PBSF before exposing (180 s) to 100 nM
598 SARS-CoV-2 RBD (Acro Biosystems, Cat # SPD-C52H3). Last, RBD-bound sensors were
599 exposed (180 s) to 300 nM ACE2 to assess competition, where antibodies that resulted in
600 increased sensor responses after ACE2 exposure represented non-ACE2-competitive binding
601 profiles while those resulting in unchanged responses represented ACE2-competitive profiles.
602

603 Deep mutational scanning analysis of antibody binding escape.

604 Yeast-display deep mutational scanning experiments identifying mutations that escape
605 binding by each monoclonal antibody were conducted with duplicate site-saturation mutagenesis
606 Omicron BA.1 RBD libraries (13). Yeast libraries were grown in SD-CAA media (6.7 g/L Yeast
607 Nitrogen Base, 5.0 g/L Casamino acids, 2.13 g/L MES, and 2% w/v dextrose), and backdiluted
608 to 0.67 OD600 in SG-CAA+0.1%D (SD-CAA with 2% galactose and 0.1% dextrose in place of
609 the 2% dextrose) to induce RBD expression, which proceeded for 16-18 hours at room
610 temperature with mild agitation. 5 OD of cells were washed in PBS-BSA (0.2 mg/L) and labeled
611 for one hour at room temperature in 1 mL with a concentration of antibody determined as the
612 EC90 from pilot isogenic binding assays. In parallel, 0.5 OD of yeast expressing the Omicron
613 BA.1 wildtype RBD were incubated in 100 µL of antibody at the matched EC90 concentration or
614 0.1x the concentration for FACS gate-setting. Cells were washed, incubated with 1:100 FITC-
615 conjugated chicken anti-Myc antibody (Immunology Consultants CMYC-45F) to label RBD
616 expression and 1:200 PE-conjugated goat anti-human-IgG (Jackson ImmunoResearch 109-115-
617 098) to label bound antibody. Labeled cells were washed and resuspended in PBS for FACS.

618 Antibody-escape cells in each library were selected via FACS on a BD FACSAria II.
619 FACS selection gates were drawn to capture approximately 50% of yeast expressing the
620 wildtype BA.1 RBD labeled at 10x reduced antibody labeling concentration (see gates in Fig.
621 S10A). For each sample, ~4 million RBD⁺ cells were processed on the sorter with collection of
622 cells in the antibody-escape bin. Sorted cells were grown overnight in SD-CAA + pen-strep,
623 plasmid purified (Zymo D2005), PCR amplified, and barcode sequenced on an Illumina
624 NextSeq. In parallel, plasmid samples were purified from 30 OD of pre-sorted library cultures
625 and sequenced to establish pre-selection barcode frequencies.

626 Demultiplexed Illumina barcode reads were matched to library barcodes in barcode-
627 mutant lookup tables using dms_variants (version 0.8.9), yielding a table of counts of each
628 barcode in each pre- and post-sort population which is available at

629 https://github.com/jbloomlab/SARS-CoV-2-RBD_Omicron_MAP_Adimab/blob/main/results/counts/variant_counts.csv.gz. The escape
630 fraction of each barcoded variant was computed from sequencing counts in the pre-sort and
631 antibody-escape populations via the formula:

$$633 E_v = F * \left(\frac{n_v^{post}}{N^{post}} \right) / \left(\frac{n_v^{pre}}{N^{pre}} \right)$$

634 where F is the total fraction of the library that escapes antibody binding, n_v is the counts of
635 variant v in the pre- or post-sort samples with a pseudocount addition of 0.5, and N is the total

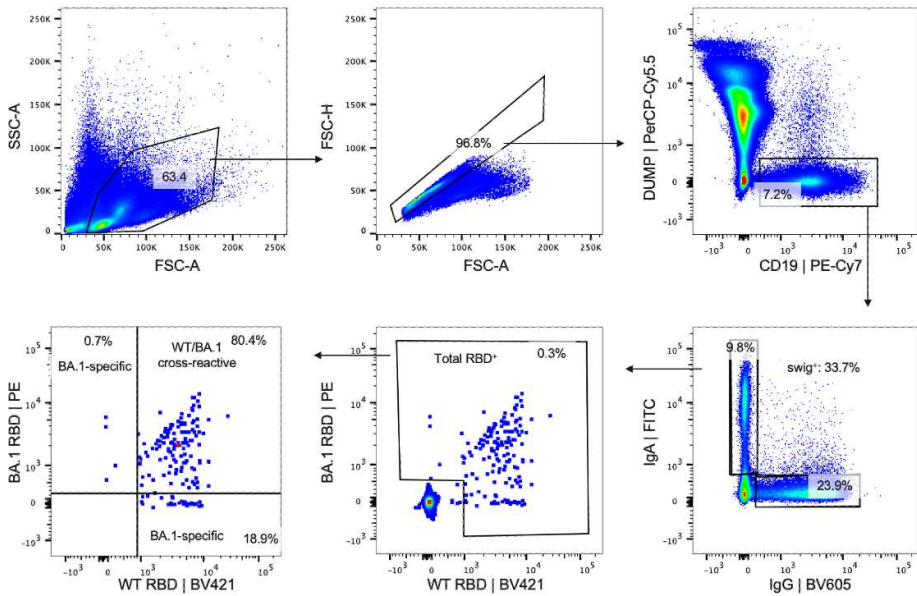
636 sequencing count across all variants pre- and post-sort. These escape fractions represent the
637 estimated fraction of cells expressing a particular variant that fall in the escape bin. Per-barcode
638 escape scores are available at https://github.com/jbloomlab/SARS-CoV-2-RBD_Omicron_MAP_Adimab/blob/main/results/escape_scores/scores.csv.

640 We applied computational filters to remove mutants with low sequencing counts or
641 highly deleterious mutations that had ACE2 binding scores < -2 or expression scores of < -1 ,
642 and we removed mutations to the conserved RBD cysteine residues. Per-mutant escape fractions
643 were computed as the average across barcodes within replicates, with the correlations between
644 replicate library selections shown in Fig. S10B. Final escape fraction measurements averaged
645 across replicates are available at https://github.com/jbloomlab/SARS-CoV-2-RBD_Omicron_MAP_Adimab/blob/main/results/supp_data/Adimabs_raw_data.csv.

646

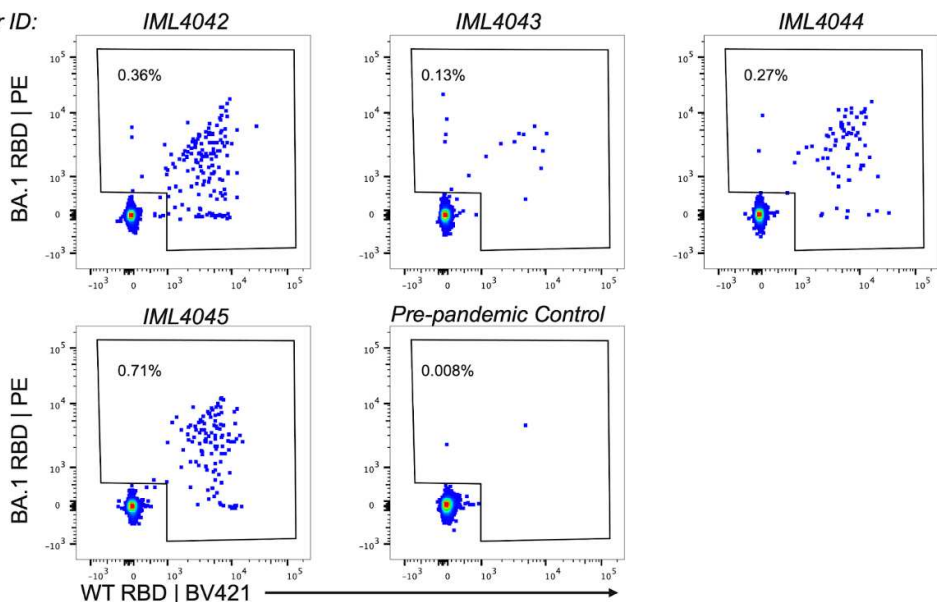
647 **Supplementary Figures:**

A



B

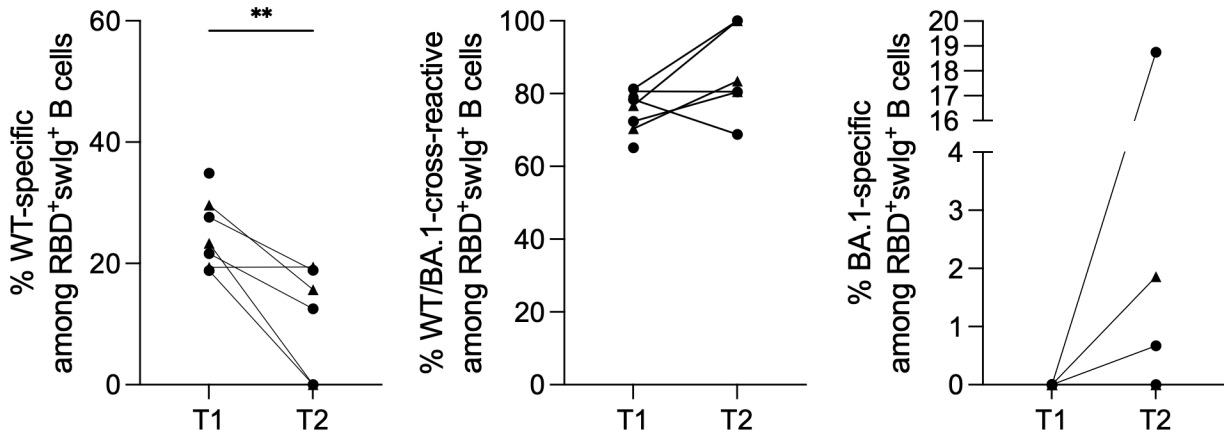
Donor ID:



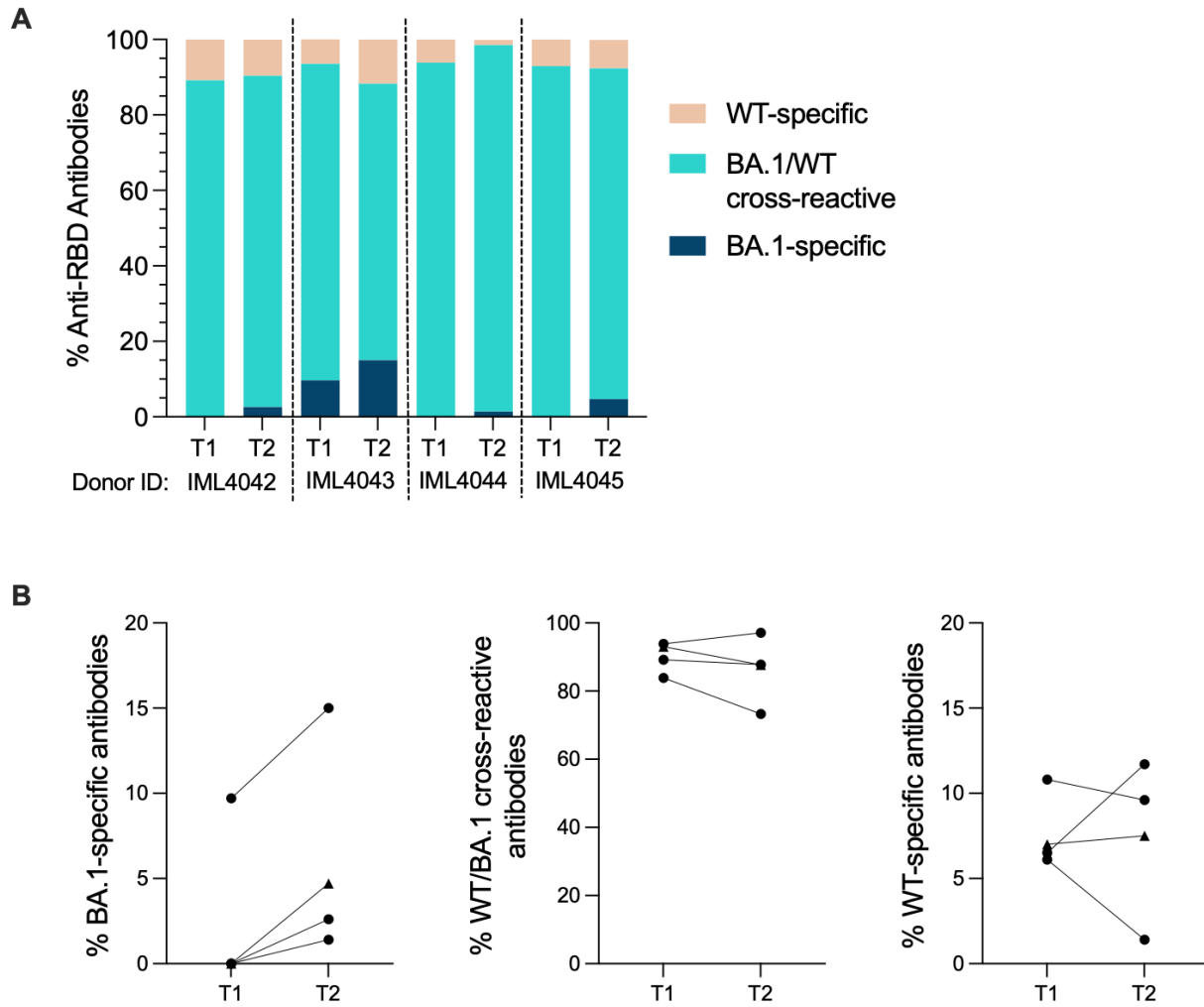
648

649

650 **Fig. S1. SARS-CoV-2 antigen-specific B cell staining and sorting.** (A) Representative FACS
651 gating strategy to determine frequencies of WT and/or BA.1 RBD-reactive B cells among class-
652 switched (IgG⁺ or IgA⁺) B cells. The frequency of events in each gate relative to the parent gate
653 are shown as percentages in each plot. (B) FACS gates used for single-cell sorting of WT and/or
654 Omicron BA.1 RBD-specific memory B cells in 4 individuals 5-6 months following BA.1
655 breakthrough infection, Donors IML4042, IML4043, and IML4044 experienced breakthrough
656 infection following two-dose mRNA vaccination, and IML4045 was infected after a third mRNA
657 dose. A healthy pre-pandemic donor sample is shown as a control. FSC-A, forward scatter area;
658 FSC-H, forward scatter height; swIg⁺, class-switched immunoglobulin; SSC-A, side scatter area.

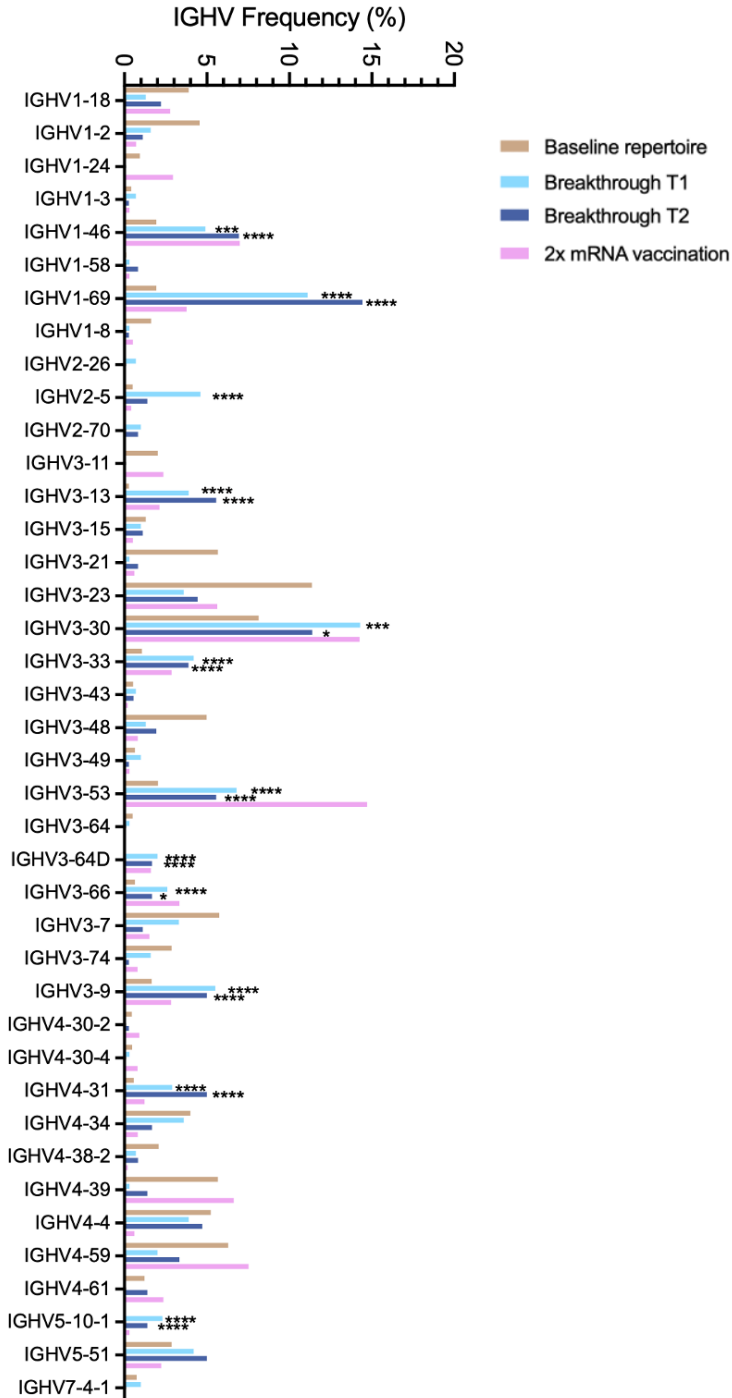


659
660
661 **Fig. S2. Cross-reactivity of RBD-directed B cells at early and late time points following**
662 **BA.1 breakthrough infection.** Proportion of RBD-directed class-switched B cells that are (left)
663 WT-specific, (middle) WT/BA.1 cross-reactive, and (right) BA.1-specific at 1-month (T1) and 5-
664 6-month (T2) time points, as determined by flow cytometry. Donors infected after two-dose
665 mRNA vaccination (n = 4) are shown as circles and those infected after a third mRNA booster
666 dose (n = 3) are shown as triangles. One two-dose vaccinated breakthrough donor was censored
667 at the second time point. Statistical comparisons were determined by Mann-Whitney U tests. **P
668 < 0.01.



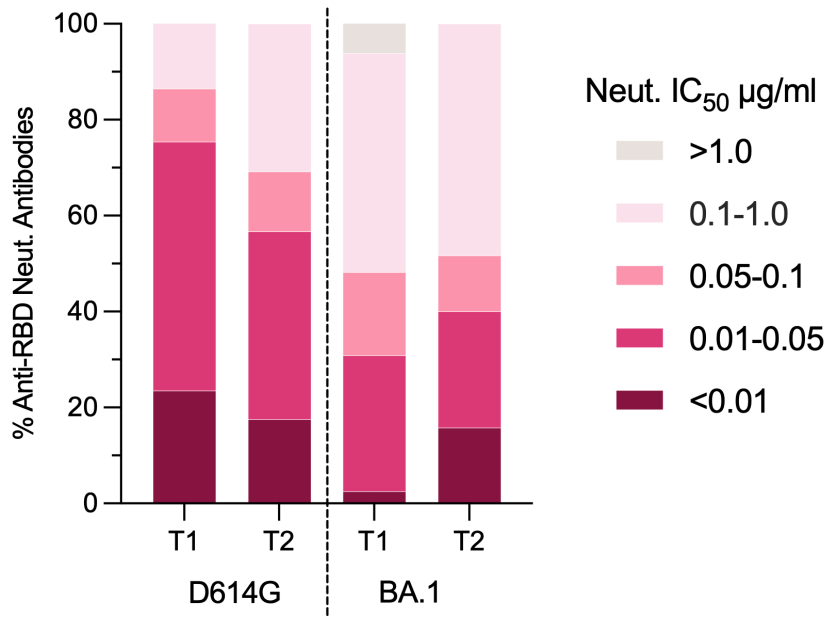
669
670
671
672
673
674
675
676
677
678

Fig. S3. Cross-reactivity of RBD-directed monoclonal antibodies isolated at 1- and 5-6 months following BA.1 breakthrough infection. (A-B) Proportion of BA.1-specific, WT-specific, and WT/BA.1 cross-reactive antibodies isolated from breakthrough infection donors at 1-month (T1) and 5-6-month (T2) time points, as determined by BLI. **(B)** Summary of antibody cross-reactivity at both time points. Connected data points represent paired samples for each donor. Donors infected after two-dose mRNA vaccination (n = 4) are shown as circles and those infected after a third mRNA booster dose (n = 3) are shown as triangles. One two-dose vaccinated breakthrough donor was censored at the second time point.



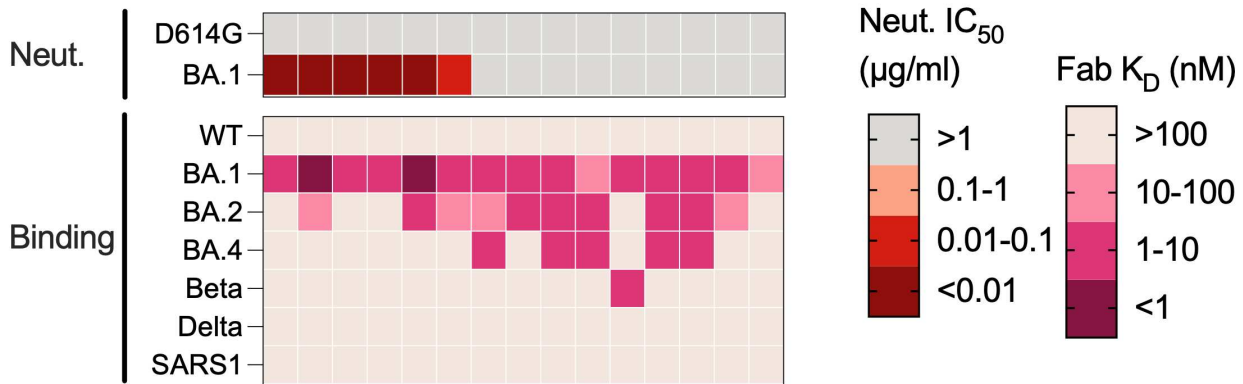
679
680
681
682
683
684
685
686
687

Fig. S4. IGHV germline usage among cross-reactive antibodies. Human IGHV germline gene usage frequencies among WT/BA.1 cross-reactive antibodies at 1 month (T1) and 5-6 month (T2) time points. Germline gene distribution of RBD-directed antibodies derived from two-dose mRNA-vaccinated/uninfected donors were obtained from the CoV-AbDab database (29). Human baseline (unselected) repertoire frequencies were included for reference (25). Statistical comparisons were made by Fisher's exact test compared to the baseline repertoire. IGHV, immunoglobulin heavy variable domain. * $P < 0.05$, ** $P < 0.01$, *** $P < 0.001$, **** $P < 0.0001$.



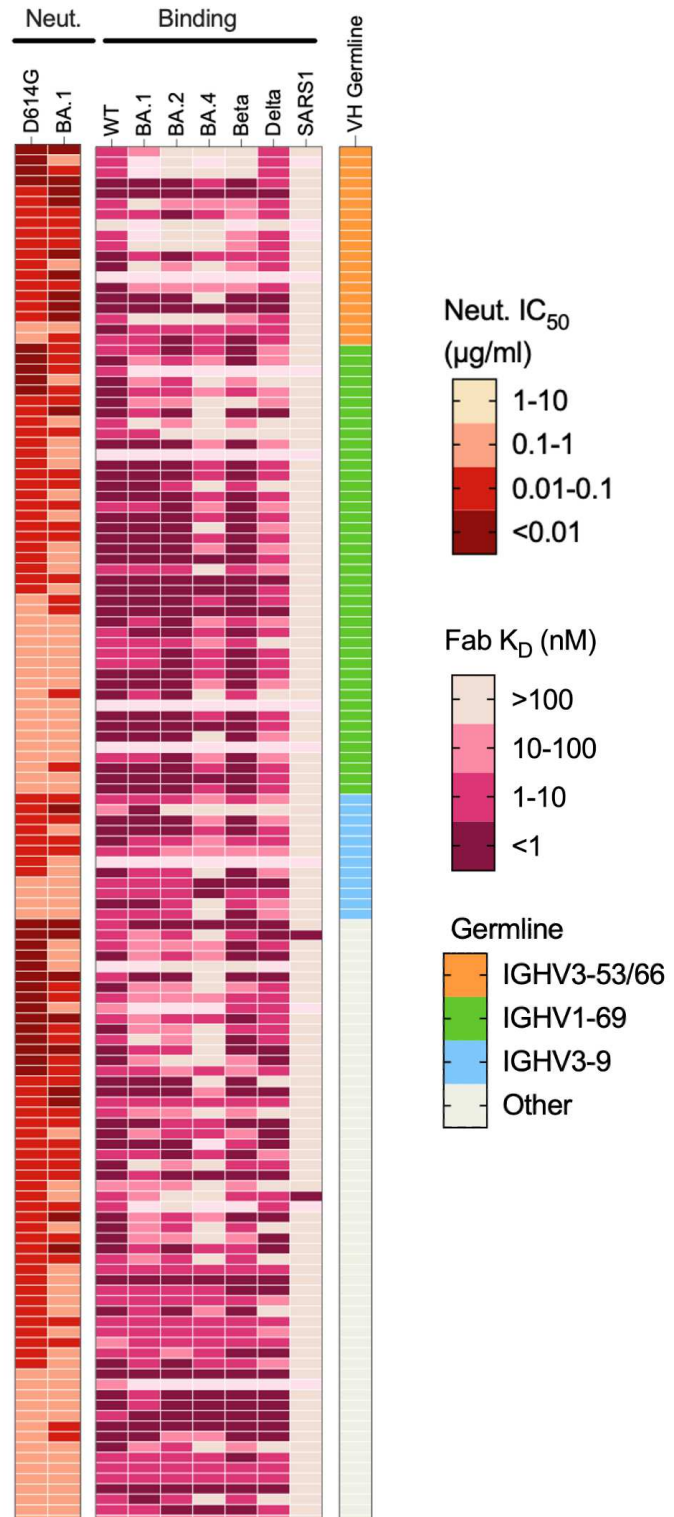
688
689
690
691
692
693
694
695

Fig. S5. Neutralization potency of D614G/BA.1 cross-neutralizing antibodies following BA.1 breakthrough infection. Proportion of antibodies isolated at the early (T1) and late (T2) time points with the indicated neutralization IC₅₀s against SARS-CoV-2 D614G and BA.1, as determined by MLV-based pseudovirus neutralization assay. Statistical comparison of BA.1 neutralizing activity by the top ten percentiles of antibodies isolated at early and late time points show significantly more potent neutralization by antibodies identified at the late time point (bootstrapping analysis of 10th percentile difference using 5,000 bootstrap iterations, $P<0.0001$).

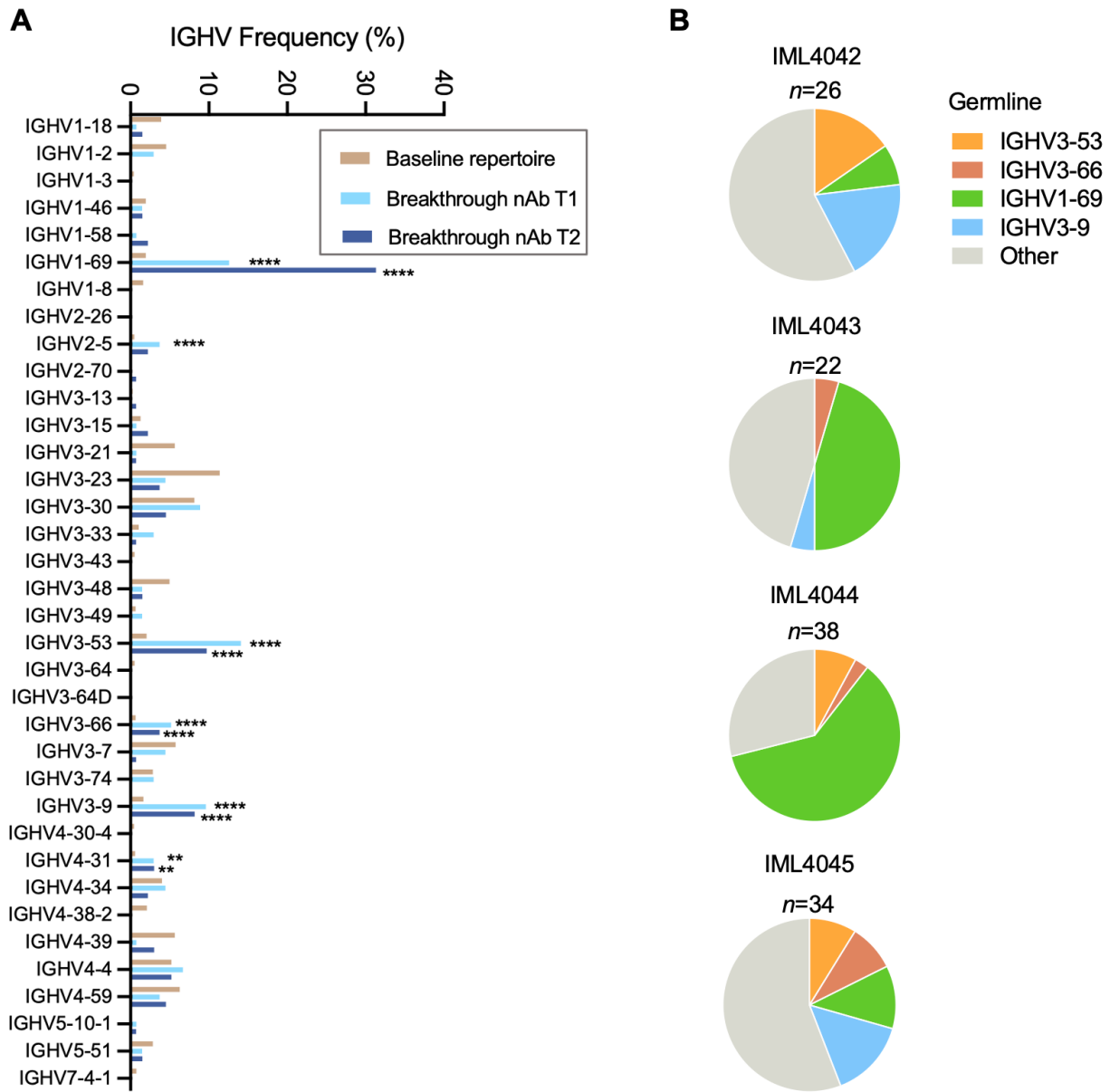


696
697
698
699

Fig. S6. Binding and neutralization properties of BA.1-specific antibodies. Heatmap showing neutralization IC₅₀s and SARS-CoV-2 variant RBD binding affinities of BA.1-specific antibodies.

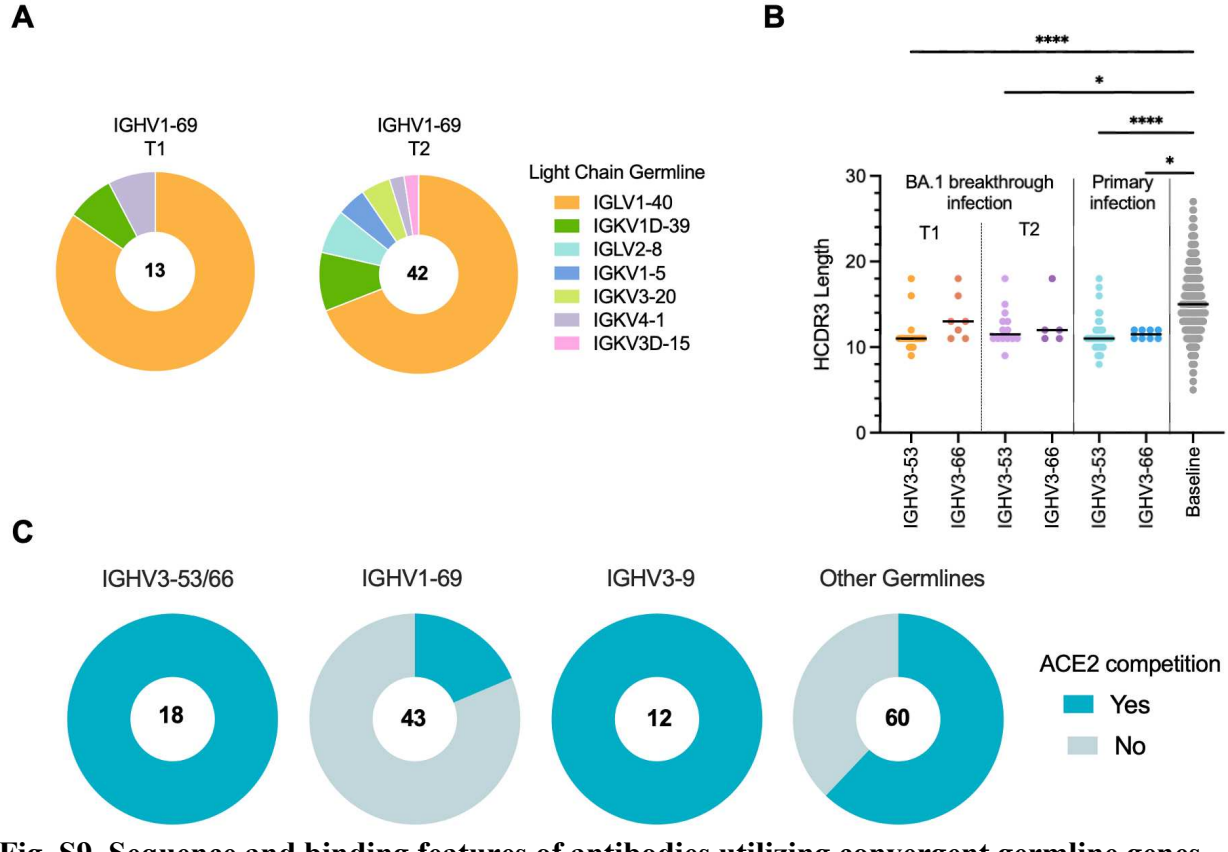


700
701 **Fig. S7. Binding breadth of D614G/BA.1 cross-neutralizing antibodies.** Heatmap showing
702 neutralization IC_{50} s and SARS-CoV-2 variant RBD binding affinities of D614G/BA.1 cross-
703 neutralizing antibodies isolated 5-6 months following BA.1 breakthrough infection. Antibodies
704 utilizing convergent germline are indicated in the right-most column.

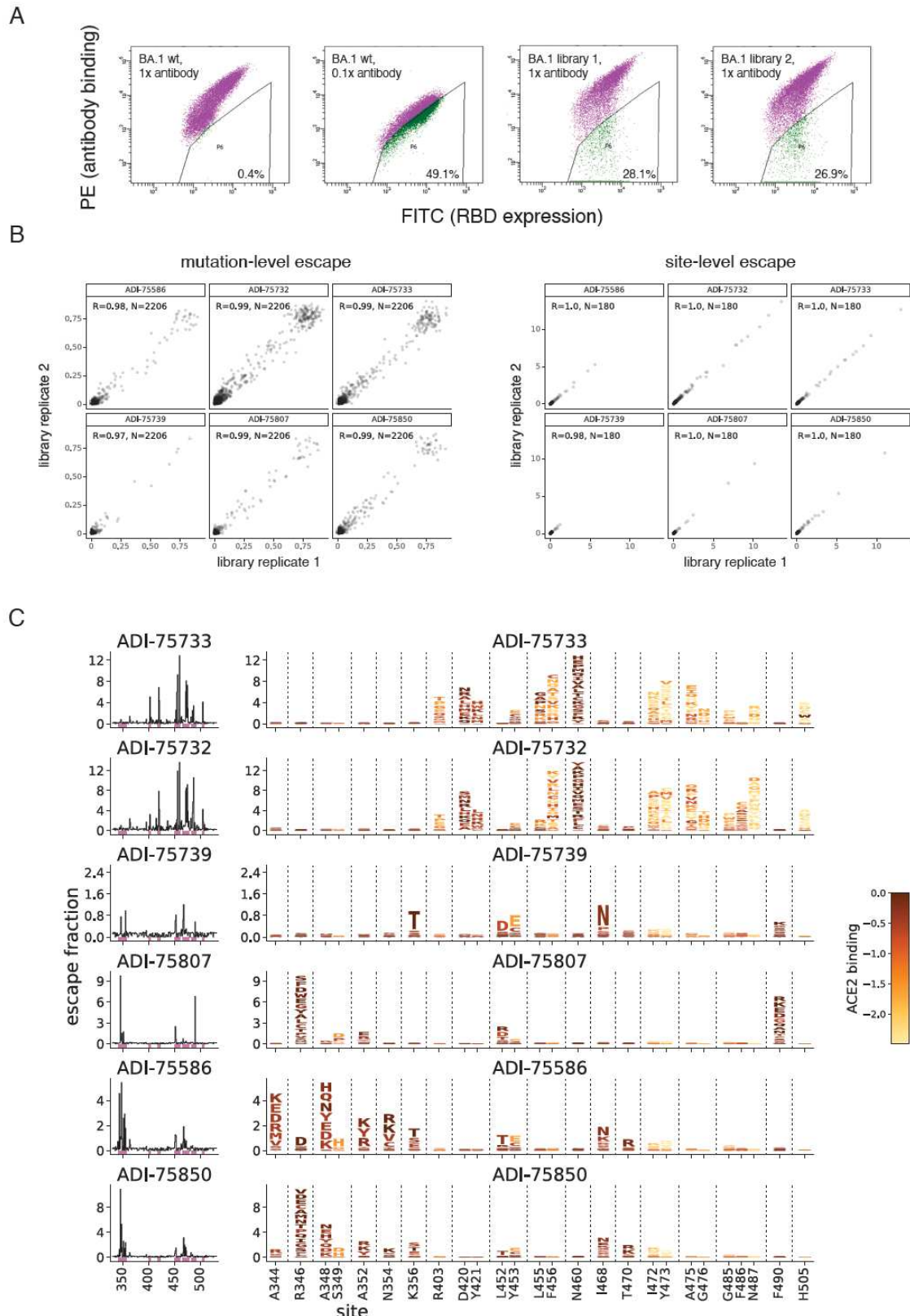


705
706
707
708
709
710
711
712
713

Fig. S8. Germline gene usage of D614G/BA.1 cross-neutralizing antibodies isolated 5-6 months following BA.1 breakthrough infection. (A) Human IGHV germline distribution frequencies among D614G/BA.1 cross-neutralizing antibodies isolated 1-month (T1) and 5-6-months (T2) following breakthrough infection, with human baseline repertoire frequencies shown for comparison (25). (B) Pie charts showing the proportion of cross-neutralizing antibodies isolated from each donor that utilize convergent germline genes. The total number of antibodies isolated from each donor is indicated above each pie chart. IGHV, immunoglobulin human variable domain; *P < 0.05, **P < 0.01, ***P < 0.001, ****P < 0.0001.



714
715 **Fig. S9. Sequence and binding features of antibodies utilizing convergent germline genes.**
716 (A) Pie charts showing light chain germline usage among *IGHV1-69* antibodies isolated at 1-
717 month (T1) and 5-6 month (T2) time points. The number of antibodies analyzed from each time
718 point is indicated in the center of each pie. (B) HCDR3 amino acid length distribution of *IGHV3-*
719 *53* and *IGHV3-66* cross-neutralizing antibodies isolated 1-month (T1) and 5-6 months (T2)
720 following BA.1 breakthrough infection. HCDR3 lengths of *IGHV3-53/3-66*-utilizing antibodies
721 isolated following primary D614G infection and the baseline human antibody repertoire were
722 included for comparison (25, 30). (C) Proportion of cross-neutralizing antibodies utilizing the
723 indicated germline genes that compete with the ACE2 receptor for binding, as determined by a
724 BLI competition assay. The number of antibodies analyzed is shown in the center of each pie.
725 Statistical comparisons were determined by Kruskal-Wallis test with subsequent Dunn's multiple
726 comparisons. A.A., amino acids; *P < 0.05; ***P < 0.0001.



727

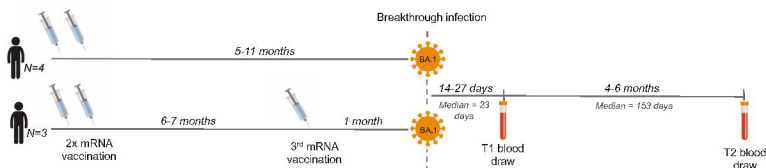
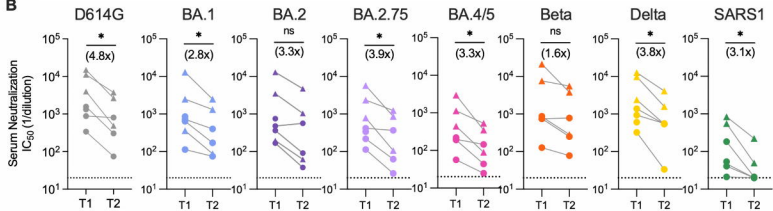
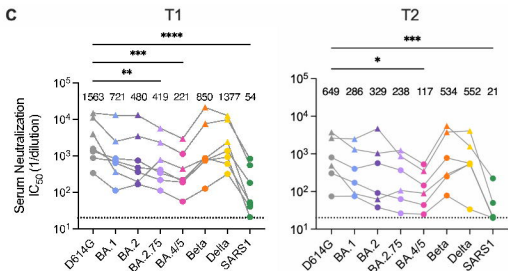
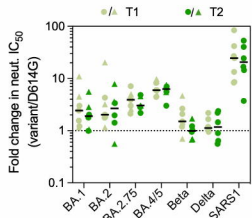
728 **Fig. S10. Deep mutational scanning analysis.** (A) Representative FACS gates used to select
729 antibody-escape mutations in yeast-displayed Omicron BA.1 mutant libraries. Gates were drawn

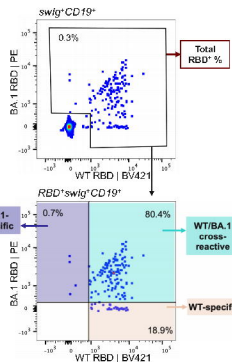
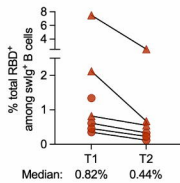
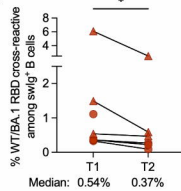
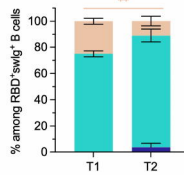
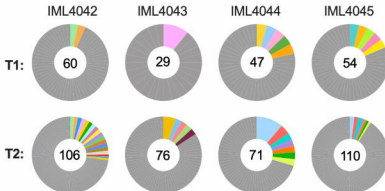
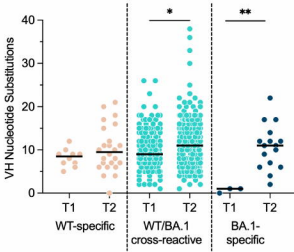
730 to capture ~50% of wildtype Omicron BA.1-expressing yeast labeled at an antibody
731 concentration 0.1x the selection concentration. From duplicate mutant libraries, yeast cells in the
732 antibody-escape bin were sorted and sequenced. Post-sort mutant frequencies were compared to
733 the pre-sort population to calculate per-mutant “escape fractions”, the fraction of cells expressing
734 a mutation that were found in the antibody-escape sort gate. (B) Correlation in per-mutation
735 (left) and per-site (right) escape fractions in replicate library selections for each antibody. (C)
736 Lineplots at left show the total site-wise escape at each RBD site. This metric is mapped to
737 structure in Fig. 3E. Sites of strong escape indicated by pink bars are shown at the mutation level
738 in logoplots at center. Mutations are colored by their effects on ACE2 binding (scale bar at
739 right). Note that prominent escape mutations such as K356T and I468N introduce N-linked
740 glycosylation motifs.

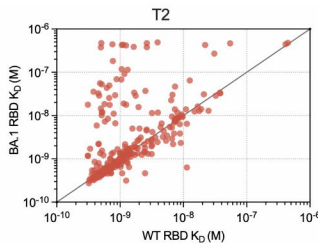
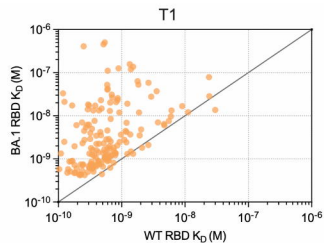
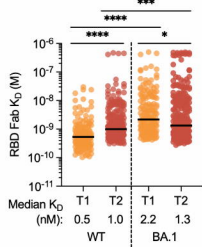
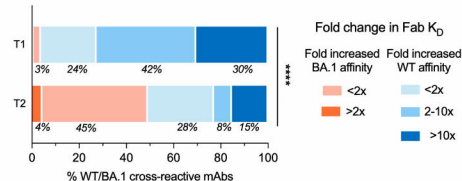
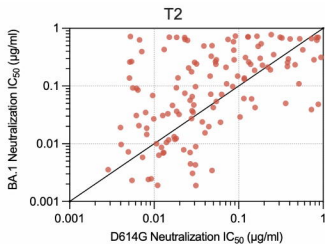
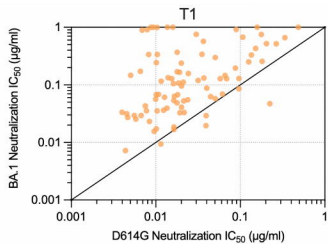
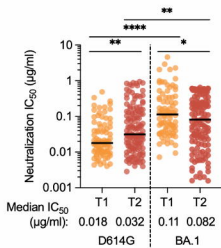
741 **Table S1. Donor Characteristics.**

| Donor ID | IML4041 | IML4042 | IML4043 | IML4044 | IML4045 | IML4054 | IML4055 |
|--|---------------|--------------|--------------|--------------|----------------------------|--------------|--------------|
| Age | 45 | 19 | 23 | 23 | 24 | 38 | 23 |
| Sex | F | F | M | F | F | F | F |
| Vaccination History | 2x BNT162b 2 | 2x BNT162b 2 | 2x BNT162b 2 | 2x BNT162b 2 | 2x BNT162b 2, 1x mRNA-1273 | 3x mRNA-1273 | 3x BNT162b 2 |
| Date of 2nd vaccination dose | 7-May-21 | 22-Jul-21 | 23-May-21 | 10-Feb-21 | 15-May-21 | 5-May-21 | 1-May-21 |
| Date of 3rd dose (if applicable) | - | - | - | - | 20-Dec-21 | 11-Dec-21 | 9-Dec-21 |
| Date of infection | 31-Dec-21 | 4-Jan-22 | 30-Dec-21 | 2-Jan-22 | 6-Jan-22 | 19-Jan-22 | 6-Jan-22 |
| Days between infection and first (T1) sample collection | 25 | 21 | 26 | 23 | 19 | 14 | 27 |
| Days between infection and second (T2) sample collection | N/A; censored | 170 | 139 | 139 | 168 | 122 | 168 |

742

A**B****C****D**

A**B****C****D****E****F**

A**B****C****D****E****F**